Kawaguchi T, Itou M, Taniguchi E, Sata M	Exendin-4, a glucagon-like peptide-1 receptor agonist, modulates hepatic fatty acid composition and Δ-5-desaturase index in a murine model of non-alcoholic steatohepatitis	Int J Mol Med	34(3)	782-787	2014
Yamada S, Kawaguchi A, Kawaguchi T, Fukushima N, Kuromatsu R, Sumie S, Takata A, Nakano M, Satani M, Tonan T, Fujimoto K, Shima H, Kakuma T, Torimura T, Charlton MR, Sata M	Serum albumin level is a notable profiling factor for non-B, non-C hepatitis virus-related hepatocellular carcinoma: A data-mining analysis	Hepatol Res	44(8)	837-845	2014
Fukuhara T, Wada M, Nakamura S, Ono C, Shiokawa M, Yamamoto S, Motomura T, Okamoto T, Okuzaki D, Yamamoto M, Saito I, Wakita T, Koike K, and Matsuura Y.	Amphipathic α-Helices in apolipoproteins are crucial to the formation of infectious hepatitis C virus particles.	PLoS Pathog		doi: 10.1371/journal.ppat.1004534	201 4
Shiokawa M, Fukuhara T, Ono C, Yamamoto S, Okamoto T, Watanabe N, Wakita T, and Matsuura Y.	Novel permissive cell lines for a complete propagation of hepatitis C virus.	J Virol	88	5578-5594	2014
Ratnoglik, SL., Jang, DP., Aoki, C., Sudarmono, P., Shoji, I., Deng, L., and Hotta, H.	Induction of cell-mediated immune responses in mice by DNA vaccines that express hepatitis C virus NS3 mutants lacking serine protease and NTPase/RNA helicase activities.	PLoS One	9	e98877	2014
Ratnoglik, SL., Aoki, C., Sudarmono, P., Komoto, M., Deng, L., Shoji, I., Fuchino, H., Kawahara, N., and Hotta, H.	Antiviral activity of extracts from Morinda citrifolia leaves and chlorophyll catabolites pheophorbide a and pyropheophorbide a, against hepatitis C virus.	Microbiology and Immunology	58	188-194	2014
Adianti, M., Aoki, C., Komoto, M., Deng, L., Shoji, I., Wahyuni, T., Lusida, M., Soetjipto, S., Fuchino, H., Kawahara, N., and Hotta, H.	Anti-hepatitis C virus compounds obtained from Glycyrrhiza uralensis and other Glycyrrhiza species.	Microbiology and Immunology	58	180-187	2014
Tao RR, Huang JY, Lu YM, Hong LJ, Wang H, Masood MA, Ye WF, Zhu DY, Huang Q, Fukunaga K, Lou YJ, Shoji I, Wilcox CS, Lai EY, Han F.	Nitrosative stress induces peroxiredoxin 1 ubiquitination during ischemic insult via E6AP activation in endothelial cells both in vitro and in vivo.	Antioxidants & Redox Signaling	21	1-16	2014
Sekine S, Ito K, Watanabe H, Nakano T, Moriya K, Shintani Y, Fujie H, Tsutsumi T, Miyoshi H, Fujinaga H, Shinzawa S, Koike K, Horie T.	Mitochondrial iron accumulation exacerbates hepatic toxicity caused by hepatitis C virus core protein.	Toxicol Appl Pharmacol.	Dec 27;282(3):237-243	237-243	2014

Yamada N, Shigefuku R, Sugiyama R, Kobayashi M, Ikeda H, Takahashi H, Okuse C, Suzuki M, Itoh F, Yotsuyanagi H, Yasuda K, Moriya K, Koike K, Wakita T, Kato T.	Acute hepatitis B of genotype H resulting in persistent infection.	World J Gastroenterol.	Mar 21;20(11):	3044-9	2014
Nguyen T, Xu J, Chikuma S, Hiai H, Kinoshita K, Moriya K, Koike K, Marcuzzi GP, Pfister H, Honjo T, Kobayashi M.	Activation-induced cytidine deaminase is dispensable for virus-mediated liver and skin tumor development in mouse models.	Int Immunol.	26(7):	397-406	2014
Horiuchi Y, Takagi A, Kobayashi N, Moriya O, Nagai T, Moriya K, Tsutsumi T, Koike K, Akatsuka T.	Effect of the infectious dose and the presence of hepatitis C virus core gene on mouse intrahepatic CD8 T cells.	Hepatol Res.	44 (10)	240-252	2014
Nakagawa H, Fujiwara N, Tateishi R, Arano T, Nakagomi R, Kondo M, Minami T, Sato M, Uchino K, Enooku K, Asaoka Y, Kondo Y, Shiina S, Yoshida H, Koike K.	Serum Levels of Interleukin-6 and Adiponectin on All-Cause, Liver-Related, and Liver-Unrelated Mortality in Chronic Hepatitis C Patients	J Gastroenterol Hepatol	30(2)	379-88	2015
Tateishi R, Okanoue T, Fujiwara N, Okita K, Kiyosawa K, Omata M, Kumada H, Hayashi N, Koike K.	Clinical Characteristics, Treatment, and Prognosis of Non-B, Non-C Hepatocellular Carcinoma: A Large Retrospective Multicenter Cohort Study.	J Gastroenterol	[Epub]		2014
Sato M, Kato N, Tateishi R, Muroyama R, Kowatari N, Li W, Goto K, Otsuka M, Shiina S, Yoshida H, Omata M, Koike K.	Impact of Pnpla3 Polymorphisms on the Development of Hepatocellular Carcinoma in Patients with Chronic Hepatitis C Virus Infection.	Hepatol Res	44(10)	E137-44	2014
Fujiwara N, Tateishi R, Nakagawa H, Nakagomi R, Kondo M, Minami T, Sato M, Uchino K, Enooku K, Kondo Y, Asaoka Y, Shiina S, Yoshida H, Koike K	Slight Elevation of High-Sensitivity C-Reactive Protein to Predict Recurrence and Survival in Patients with Early Stage Hepatitis C-Related Hepatocellular Carcinoma	Hepatol Res	[Epub]		2014

DNA methylation at hepatitis B viral integrants is associated with methylation at flanking human genomic sequences

Yoshiyuki Watanabe,[1,2,9] Hiroyuki Yamamoto,[1,9] Ritsuko Oikawa,[1] Minoru Toyota,[3] Masakazu Yamamoto,[4] Norihiro Kokudo,[5] Shinji Tanaka,[6] Shigeki Arii,[6] Hiroshi Yotsuyanagi,[7] Kazuhiko Koike,[8] and Fumio Itoh[1]

[1]*Division of Gastroenterology and Hepatology, Department of Internal Medicine, St. Marianna University School of Medicine, Kawasaki 216-8511, Japan;* [2]*Internal Medicine, Kawasaki Rinko General Hospital, Kawasaki 210-0806, Japan;* [3]*Department of Molecular Biology, Sapporo Medical University School of Medicine, Sapporo 060-8556, Japan;* [4]*Department of Surgery, Institute of Gastroenterology, Tokyo Women's Medical University, Tokyo 162-8666, Japan;* [5]*Hepato-Biliary-Pancreatic Surgery Division, Artificial Organ and Transplantation Division, Department of Surgery, Graduate School of Medicine, University of Tokyo 113-8655, Japan;* [6]*Department of Hepatobiliary Pancreatic Surgery, Graduate School, Tokyo Medical and Dental University, Tokyo 113-0034, Japan;* [7]*Department of Infectious Diseases, Graduate School of Medicine, University of Tokyo, Tokyo 113-8655, Japan;* [8]*Department of Gastroenterology, Graduate School of Medicine, University of Tokyo, Tokyo 113-8655, Japan*

Integration of DNA viruses into the human genome plays an important role in various types of tumors, including hepatitis B virus (HBV)–related hepatocellular carcinoma. However, the molecular details and clinical impact of HBV integration on either human or HBV epigenomes are unknown. Here, we show that methylation of the integrated HBV DNA is related to the methylation status of the flanking human genome. We developed a next-generation sequencing-based method for structural methylation analysis of integrated viral genomes (denoted G-NaVI). This method is a novel approach that enables enrichment of viral fragments for sequencing using unique baits based on the sequence of the HBV genome. We detected integrated HBV sequences in the genome of the PLC/PRF/5 cell line and found variable levels of methylation within the integrated HBV genomes. Allele-specific methylation analysis revealed that the HBV genome often became significantly methylated when integrated into highly methylated host sites. After integration into unmethylated human genome regions such as promoters, however, the HBV DNA remains unmethylated and may eventually play an important role in tumorigenesis. The observed dynamic changes in DNA methylation of the host and viral genomes may functionally affect the biological behavior of HBV. These findings may impact public health given that millions of people worldwide are carriers of HBV. We also believe our assay will be a powerful tool to increase our understanding of the various types of DNA virus-associated tumorigenesis.

[Supplemental material is available for this article.]

Hepatitis B virus (HBV) infects more than two billion people worldwide, and 400 million chronically infected individuals are at high risk of developing active hepatitis, cirrhosis, and hepatocellular carcinoma (HCC) (Gatza et al. 2005; Lupberger and Hildt 2007). HBV carriers with chronic liver disease are at a 100-fold greater risk of developing HCC, which is the third leading cause of cancer-related death worldwide. The HBV genome is integrated into the host genome in 90% of patients with HCC (HBV-HCC) (Gatza et al. 2005; Lupberger and Hildt 2007). HBV-HCCs have been analyzed by comprehensive genome sequencing and high-resolution genome mapping (Kan et al. 2013; Li and Mao 2013; Nakagawa and Shibata 2013). Moreover, the recent deep sequencing of HBV DNA in patients with HCC revealed increased integration events, structural alterations, and sequence variations (Ding et al. 2012; Fujimoto et al. 2012; Jiang et al. 2012; Sung et al. 2012; Toh et al. 2013). A recent study identified a viral-human chimeric fusion transcript, HBx-LINE1, that functions like a long noncoding RNA to promote HCC (Lau et al. 2014). However, the molecular details and clinical impact of HBV integration on the epigenomes of human cells and HBV remain to be defined.

Methylation of exogenous DNA (including viral DNA) that is integrated into the human genome has been studied over the past decade (Doerfler et al. 2001). Within the human genome, cytosine methylation in CpG dinucleotides (CpG sites), which cluster into islands associated with transcriptional promoters, is an important mechanism for regulating gene expression. Additionally, host cells use methylation as a defense mechanism against foreign agents (e.g., viral DNA) (Doerfler 2008; Doerfler et al. 2001). DNA methylation suppresses the expression of viral genes and other deleterious elements incorporated into the host genome over time. Establishment of de novo patterns of DNA methylation is char-

[9]**These authors contributed equally to this work.**
Corresponding author: h-yama@marianna-u.ac.jp.
Article published online before print. Article, supplemental material, and publication date are at http://www.genome.org/cgi/doi/10.1101/gr.175240.114.

25:328–337 Published by Cold Spring Harbor Laboratory Press; ISSN 1088-9051/15; www.genome.org

acterized by the gradual spread of methylation (Orend et al. 1991). Another attractive possibility is that DNA methylation camouflages the virus from the immune system (Tao and Robertson 2003; Hilleman 2004), resulting in a DNA methylation–related blockade of viral antigen presentation that allows the virus to escape immune control (Fernandez et al. 2009).

The DNA methylome of HBV in human cells may undergo dynamic changes at different stages of disease (Fernandez et al. 2009). For example, DNA methylation at the *HBVgp2* locus, which codes for the S viral proteins, reportedly increases during the progression from asymptomatic lesions to benign lesions, to premalignant disease and malignant tumors. However, because of the significant deletions of the integrated HBV genome detected in this previous study (Fernandez et al. 2009), the DNA methylome of HBV needs to be further characterized. Moreover, the molecular mechanisms involved and the clinical impact of the integration of HBV on the human and HBV epigenomes are unknown. To address these issues, we developed a next-generation sequencing (NGS)–based method for methylation analysis of integrated viral genomes (denoted G-NaVI) and applied this method to the integrative genomic and epigenomic analysis of human hepatoma cell lines and tissues with integrated HBV genomes.

Results

DNA methylation levels in PLC/PRF/5 cells and cancerous tissues obtained from HBV-HCC patients

Methylated CpG island (CGI) amplification (MCA) coupled with microarray (MCAM) analysis (Toyota et al. 1999; Oishi et al. 2012) was performed to detect methylated genes in the human PLC/PRF/5 cell line and in six paired specimens of primary HBV-HCC and adjacent tissues. Compared with the DNA methylation of CGIs in the healthy peripheral blood leukocytes of volunteers or the noncancerous tissues, levels of DNA methylation were not remarkable in the PLC/PRF/5 cells and the cancerous tissues obtained from HBV-HCC patients (Supplemental Fig. 1). These results were confirmed by bisulfite pyrosequencing of candidate tumor-related genes.

DNA methylation of CGIs of *HBx*

We then focused on epigenetic changes in the viral genome. Based on the hidden Markov models for sequence analysis performed on the CpG plugin of bioinformatics software Geneious 5.5.8 (see Methods section), a CpG island was found in only the promoter region of the *HBx* gene in the HBV genome (Fig. 1A; Supplemental Fig. 2; Durbin et al. 1998; Kearse et al. 2012). Host signal transduction pathways and gene expression are disrupted by the expression of *trans*-activating factors derived from the HBV genome, such as the HBx protein and PreS2 activators (Gatza et al. 2005; Lupberger and Hildt 2007). Moreover, transgenic mice expressing high levels of HBx in the liver develop HCC (Kim et al.1991; Koike et al. 1994). The DNA methylation levels of the CGIs of *HBx* were analyzed in 10 HBV-HCC samples and 10 adjacent samples, as well as samples of PLC/PRF/5 cells by bisulfite pyrosequencing (Fig. 1A; Supplemental Fig. 2). We performed advanced methylation quantification in long sequence runs by pyrosequencing on PyroMark Q24 Advanced and PyroMark Q24 instruments. Methylation levels of *HBx* varied across samples (Fig. 1B,C) and were generally lower in HCC tissues than in the adjacent tissues (Fig. 1B). This finding is consistent with a previous report that most HBV genomes, although globally methylated to a greater extent in malignant samples than in premalignant lesions, retain *HBx* in an unmethylated state (Fernandez et al. 2009). Because the pyrosequencing results represent the genome-wide average of DNA methylation levels at the particular CpG site, the results could be affected by the HBV integration site. Therefore, genome-wide methylation analysis of the integrated HBV sequence is necessary in relation to the methylation state of the adjacent human genome. We did not detect an association between *HBx* methylation levels and those of the LINE1 and *Alu*Yb8 repeats (Fig. 1B).

Fluorescence in situ hybridization (FISH) and *Alu* PCR analyses of HBV integration

We developed a FISH technique for detecting HBV DNA in the genome of PLC/PRF/5 cells (Supplemental Figs. 3, 4). Twelve specific primer pairs (FISH probes 1–12) were designed based on the HBV sequences integrated into the genome of PLC/PRF/5 cells; amplification from all primer pairs was confirmed (Supplemental Fig. 4A). These results suggest full-length or partial HBV sequences that are covered by the 12 primer pairs were integrated into the genome of the PLC/PRF/5 cells. The FISH probes were labeled with digoxigenin, and FISH was performed using Carnoy-fixed chromosomal and nuclear specimens. Multiple HBV fluorescent signals (green) were detected in the nuclei (Supplemental Fig. 4B) using probes for *HBx* and its CGI sequences (probes 5 and 6), but not with probes 1–4 or 7–12 (Supplemental Fig. 4C–E). *Alu*-PCR identified one *HBx* integration site in PLC/PRF/5 (Supplemental Fig. 5). The integrated *HBx* sequence was 213 bp and included a promoter region. The *HBx* gene body was located only 13 bases (ATG GCT GCT AGG T) from the transcription start site and was integrated into a noncoding region of the host genome. There were 200 bases of viral DNA sequence upstream of the *HBx* transcription start site. According to the human genome reference sequence (GRCh38) published by the Genome Reference Consortium, this integration site was identified as a noncoding region of host Chromosome 5 1,350,106–1,350,478 that is near the telomerase reverse transcriptase (*TERT*) gene (Supplemental Fig. 5).

NGS analysis of HBV DNA integration site sequences

We developed an NGS analysis technique for sequencing the HBV DNA integration sites (Supplemental Fig. 6A). For efficient genome analysis, we synthesized 12,391 custom baits based on the sequences of the HBV genotypes A to J and on those sequences present in the HBV-transformed PLC/PRF/5 cells that were not related to the human genome sequence (Supplemental Fig. 6B). The average read length was 333.14 bp with a modal length of ~500 bp (Supplemental Fig. 6C). The average read quality was 31.91, corresponding to >99.9% accuracy. We did not detect a common HBV integration site (Fig. 2). The integration sites in the PLC/PRF/5 genome included intergenic (39%), intronic (39%), promoter (8%), and divergent promoter (15%) regions but not exonic (0%) sequences (Fig. 2). HepG2.2.15 cells, which stably express and replicate HBV in a culture system, are derived from the human hepatoblastoma cell line HepG2 (Sells et al. 1987). In the HepG2.2.15 genome, the integration sites included intergenic (29%), intronic (57%), and other (14%) regions but not promoter (0%), divergent promoter (0%), or exonic (0%) sequences (Fig. 2).

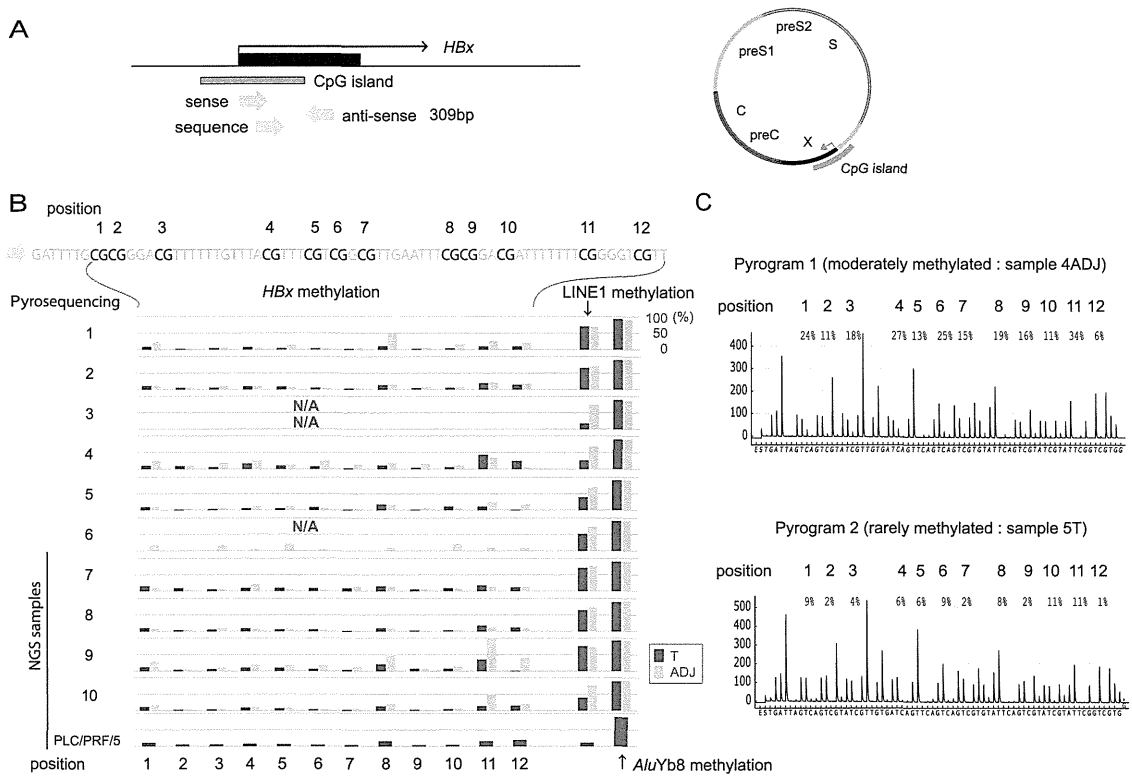

Figure 1. Methylation analysis of the CGI of the *HBx* gene. (*A*) Schema of the CGI of the *HBx* gene. Three arrows show the pyrosequencing primers used for the methylation analysis. (*B*) DNA methylation levels of the CpGs of the *HBx* gene, LINE1, and *Alu*Yb8 in 10 paired HBV-HCC and adjacent nontumor tissue samples and PLC/PRF/5 DNA were analyzed using bisulfite pyrosequencing. Methylation levels of *HBx* varied across samples and were generally lower in HCC tissues than in the adjacent nontumor tissues. An association between *HBx* methylation levels and those of the LINE1 and *Alu*Yb8 repeats was not observed. N/A, could not be analyzed. DNAs from four paired HBV-HCC and adjacent nontumor tissue samples (sample nos. 7–10), PLC/PRF5, and HepG2.2.15 were further analyzed using the NGS (G-NaVI method). (C) Representative pyrograms showing DNA methylation levels of the CpGs of the *HBx* gene. Methylation levels at 12 CpG sites of the *HBx* gene in adjacent nontumor tissue (sample no. 4ADJ) and tumor tissue (sample no. 5T) are shown.

DNA methylation of the integrated HBV genome as well as the adjacent human genome in cell lines

DNA methylation of the integrated HBV genome, as well as the adjacent human genome, was analyzed by bisulfite pyrosequencing. We detected varying levels of methylation of the HBV sequences integrated into the genome of PLC/PRF/5 cells (Fig. 3; Supplemental Fig. 7). Our data suggest DNA methylation in the integrated HBV genome is related to the methylation status of the integration sites within the human genome. We further characterized the methylation status of the HBV genome and human genome by allele-specific DNA methylation analysis (Fig. 3A), which revealed that the HBV genome often showed significant methylation when integrated into highly methylated sites in the human genome; however, the HBV genome remained largely unmethylated when integrated into unmethylated regions such as promoters (Fig. 3B). Integration of the HBV genome did not affect the methylation status of the human genome, including the promoter regions of the *TERT* and *SNX15* genes. Methylation of HBV DNA integrated into HepG2.2.15 cells transformed with HBV DNA (using a head-to-tail dimer) was further analyzed by bisulfite pyrosequencing, which revealed that the HBV genome generally showed significant methylation when integrated into highly methylated regions of the human genome; however, the HBV genome remains largely unmethylated when integrated into unmethylated regions (Fig. 3A).

DNA methylation levels in orthologous loci

We examined methylation levels of orthologous loci in HepG2.2.15 cells and in peripheral blood lymphocytes (PBLs) of a healthy volunteer and compared them to the methylation levels at the same (empty) target sites of PLC/PRF/5 cells. Methylation levels of orthologous loci in HepG2.2.15 cells and PBLs were generally similar to those of PLC/PRF/5 cells (Fig. 3B). Similarly, we examined methylation levels of orthologous loci in PLC/PRF/5 cells and in PBLs of a healthy volunteer and compared them to the methylation levels at the same (empty) target sites of HepG2.2.15 cells. Methylation levels of orthologous loci in PLC/PRF/5 cells and PBLs were also generally similar to those of HepG2.2.15 cells (Fig. 3B).

DNA methylation of the integrated HBV genome and the adjacent human genome in HCC tissues

To determine whether our results are relevant to human tumors, we used bisulfite pyrosequencing to investigate the methylation status of the HBV and human genomes in surgical specimen pairs of HCC and adjacent nontumor tissues. We detected no common HBV integration site (Fig. 4; Supplemental Fig. 8). Recurrent HBV integration into the *SLC6A13* gene was observed in cancerous tissues. Integration sites were rarely detected in exonic regions of the DNA from HBV-HCC samples (Fig. 4; Supplemental Fig. 8). Similar to the results obtained from the PLC/PRF/5 and HepG2.2.15 cells, our analysis revealed that the HBV genome became significantly

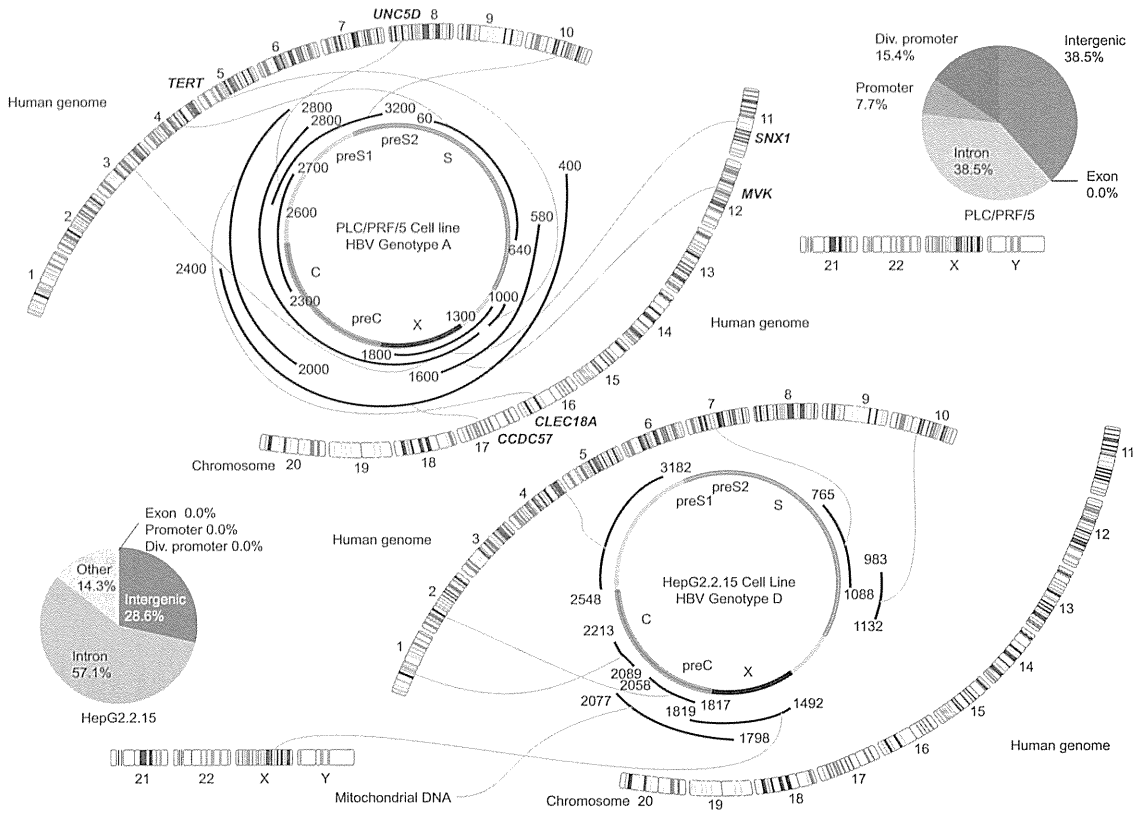

Figure 2. Distribution of the integration sites in the HBV genome and human chromosomes represented by Circos plots of the PLC/PRF/5 genome and the HepG2.2.15 genome. HBV DNA integration was analyzed using the G-NaVI method in the genome of PLC/PRF/5 cells and HepG2.2.15 cells. A common HBV integration site was not detected. Integration sites were not detected in exonic regions of the DNA from cell lines (Venn diagrams). The HBV genes (*PreC, Precore; C, Core; PreS, Presurface; S, Surface; X, X*) and the 24 human chromosomes are shown.

methylated when integrated into highly methylated human genome regions but not when integrated into unmethylated human genome regions (Fig. 4).

Correlation between the methylation pattern of the integrated HBV DNA and the human genome

DNA fragments, including 200 bp of the HBV DNA and 200 bp of the human genome around the boundary, were analyzed for average methylation, GC content, and repetitive sequences. A statistically significant correlation was observed between the average methylation of the HBV DNA and that of the human genome in cell lines and clinical samples (Fig. 5A–C; Supplemental Table 2). In contrast, average methylation did not correlate with GC content or repetitive sequences in the human and viral genome (Fig. 5D,E; Supplemental Table 2).

Using Bander software, we analyzed the chromatin structure at the integrated HBV site in PLC/PRF/5 and HepG2.2.15. Open chromatin and heterochromatin were observed more frequently at the integrated HBV in PLC/PRF/5 and HepG2.2.15, respectively (Supplemental Table 3). The difference may reflect the fact that PLC/PRF/5 is a naturally derived HBV-positive cell line and HepG2.2.15 is an HBV DNA-transfected cell line.

Discussion

We developed an NGS-based method for structural methylation analysis of integrated viral genomes. This method is a novel approach that enables the enrichment of viral fragments for sequencing using unique baits based only on the sequence of the HBV genome. We detected all regions of the human genome that harbored integrated HBV genomes without conducting unnecessary sequencing of regions where the HBV genome was not integrated. Because this technique only requires sequencing a small region of DNA around the integrated HBV sequences, a sufficient number of sequence reads can be acquired.

Methylation of viral DNA in infected cells may alter the expression patterns of viral genes related to infection and transformation (Burgers et al. 2007; Fernandez et al. 2009) and may clarify why certain infections are either cleared or persist with or without progression to precancer (Mirabello et al. 2012). To the best of our knowledge, we have, for the first time, established that the de novo patterns of DNA methylation in the integrated HBV genome are related to the methylation status of the integration sites within the human genome. A statistically significant correlation between the average methylation of the HBV DNA and that of the human genome in cell lines and clinical samples has greatly substantiated our findings. It is possible that the HBV genome becomes inactivated by methylation, when it is integrated into highly methylated host sites; therefore, HBV methylation may not contribute to tumor development. However, after integration into unmethylated human genome regions such as promoters, the HBV DNA remains unmethylated and may eventually play an important role in tumorigenesis (Fig. 6). Because multiple HBV integration sites were present in each of the analyzed samples, there remains the possibility of an asso-

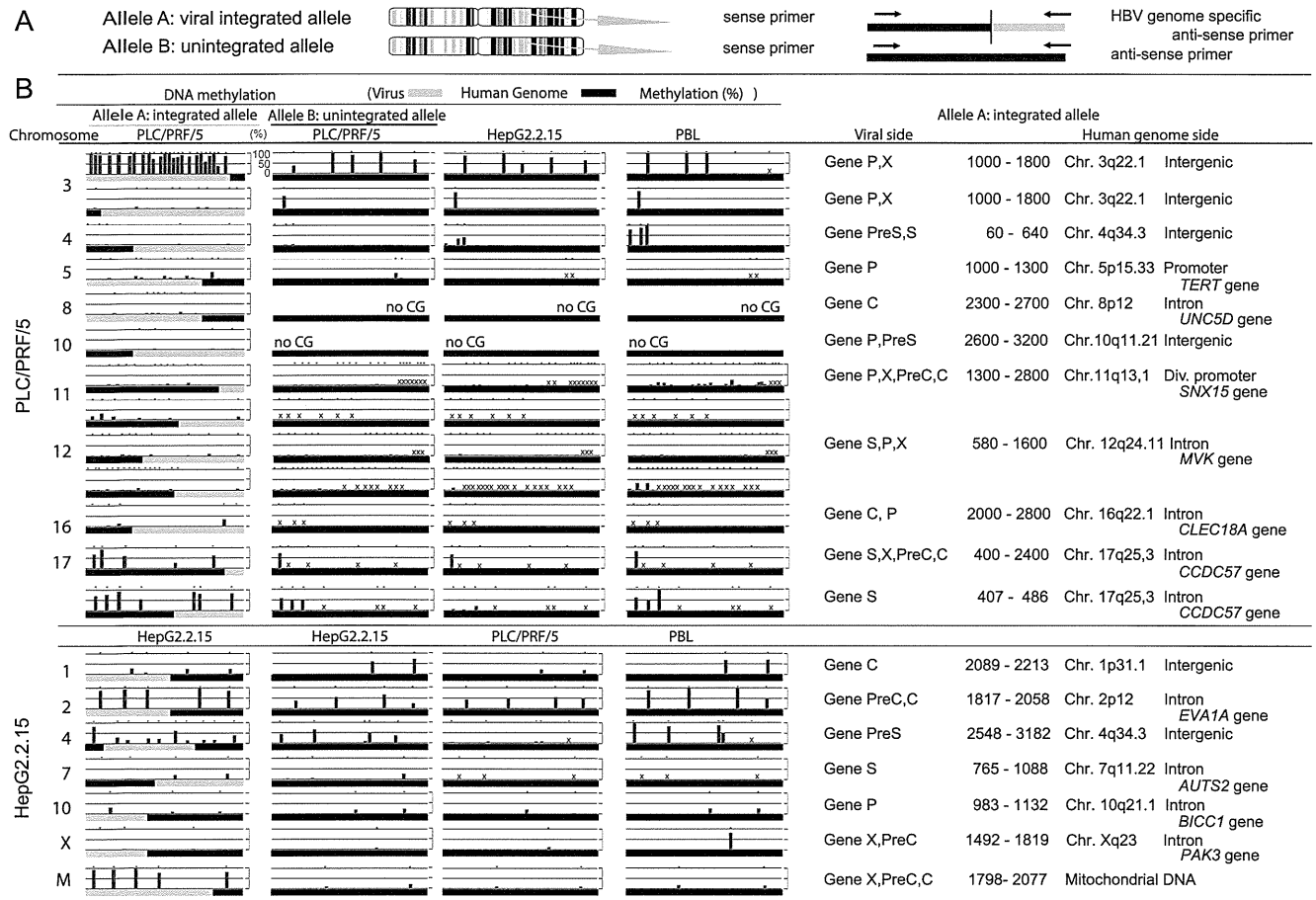

Figure 3. Allele-specific methylation analysis of the PLC/PRF/5 genome and the HepG2.2.15 genome. (*A*) A schema of allele-specific methylation analysis. (*B*) The methylation levels of the HBV and human genomes for the integrated and unintegrated alleles. Detailed results of the HBV integrants (*PreC, Precore; C, Core; PreS, Presurface; S, Surface; X, X*) and flanking host genomes (position, chromosome, location of the genome, and gene names) are shown. DNA methylation of the integrated HBV genome as well as the flanking human genome was examined by allele-specific DNA methylation analysis using bisulfite pyrosequencing. The HBV genome often showed significant methylation when integrated into highly methylated sites in the human genome; however, the HBV genome remained largely unmethylated when integrated into unmethylated regions. Methylation levels of orthologous loci in HepG2.2.15 cells and in PBLs of a healthy volunteer were examined and compared to the methylation levels at the same (empty) target sites of PLC/PRF/5 cells. Methylation levels of orthologous loci in HepG2.2.15 cells and PBLs were generally similar to those of PLC/PRF/5 cells. Similarly, methylation levels of orthologous loci in PLC/PRF/5 cells and in PBLs of a healthy volunteer were examined and compared to the methylation levels at the same (empty) target sites of HepG2.2.15 cells. Methylation levels of orthologous loci in PLC/PRF/5 cells and PBLs were generally similar to those of HepG2.2.15 cells. (×) The desired quantitative methylation levels were not obtained because of technical difficulties with the sequences that were being analyzed.

ciation between methylation and viral transcript levels. The biological impact of methylation on viral transcript levels or viral function, induced by viral insertions, also needs to be further addressed.

Methylation levels of orthologous loci in other samples at the same (empty) target sites of PLC/PRF/5 were generally similar to those of PLC/PRF/5. Similar results were observed in HepG2.2.15. These data suggest that a "before and after" relationship exists between methylation levels at preexisting target sites and those within viral insertions. At the same time, we cannot rule out the possibility that the integration of the virus subsequently affects the methylation established at the flanking target site, perhaps by acting in trans on the empty target site-containing allele. Therefore, this issue needs to be further addressed.

Differences in the integrated viral sequences could have a direct impact on the amount of cytosine methylation observed. In cases where the integration site is a highly active promoter, comparisons of methylation statuses may not be informative. Additional studies, using a large number of samples, are needed to address this issue.

Our results are notable because other studies have detected a statistically significant enrichment of HBV integration into regulatory regions, particularly promoters, in tumors (Sung et al. 2012; Toh et al. 2013); this observation may be explained by the relatively open chromatin structure of promoter regions. Average methylation did not correlate with GC content or repetitive sequences in the human and viral genomes. The relationship between methylation of HBV sequences and chromatin structure remains to be clarified because of the limitation of the Bander software used in this study. Although the mechanism needs clarification, the significant enrichment of HBV integration into regulatory regions would favor integrated HBV nonmethylation and lead to tumorigenesis. Alternatively, while the integration of HBV into the host genome may be random, HBV integration into regulatory regions is positively selected during tumorigenesis (Toh et al. 2013).

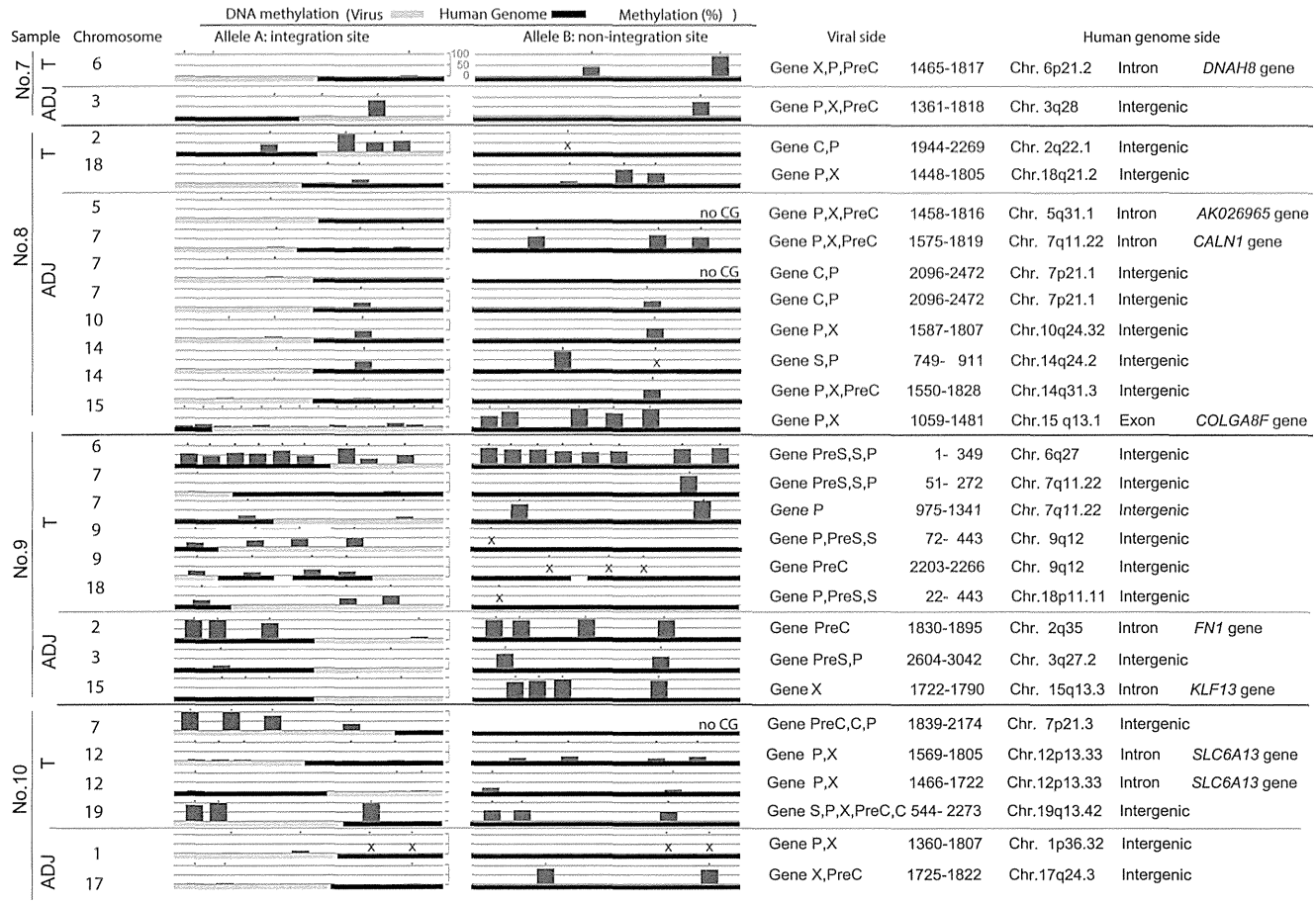

Figure 4. Allele-specific methylation analysis of the tumor (*T*) and adjacent nontumor (ADJ) sample genomes. The methylation levels of the HBV and human genomes for the integrated and unintegrated alleles in four paired tumor and adjacent nontumor samples (sample nos. 7–10) are shown. Detailed results of the HBV integrants (*PreC, Precore; C, Core; PreS, Presurface; S, Surface; X, X*) and flanking host genomes (position, chromosome, location of the genome, and gene names) are shown. The HBV genome became significantly methylated when integrated into highly methylated human genome regions, but not when integrated into unmethylated human genome regions. (×) The desired quantitative methylation levels were not obtained because of technical difficulties with the sequences that were being analyzed.

The dynamic changes in DNA methylation described here have a major functional impact on the biological behavior of HBV and underlie the molecular mechanisms that control infection or enable tumorigenesis. These findings may significantly impact public health given that millions of people worldwide are carriers of HBV. Distinct DNA methylation profiles may exist, for example, between primary HCCs in Japanese patients and those of other nationalities. Additional studies are needed to address this issue, and research into the influence of other environmental factors is required.

Increased viral DNA methylation is present in cancers associated with DNA viruses, including human papilloma virus types 16 and 18 (HPV 16 and 18) (Fernandez et al. 2009; Mirabello et al. 2012), Epstein-Barr virus (Uozaki and Fukayama 2008; Fernandez et al. 2009), and human T-lymphotropic virus 1 (Taniguchi et al. 2005). An analysis of the haplotype-resolved genome and epigenome of the aneuploid HeLa cervical cancer cell line revealed that an amplified, highly rearranged region of chromosome 8q24.21 harboring an integrated HPV18 genome likely represents the tumor-initiating event (Adey et al. 2013). Whether the dynamic changes in DNA methylation observed in cells with integrated HBV genomes also occur in human cells infected by other viruses is an interesting question for further study. We anticipate that our assay will be a powerful tool for this purpose and have successfully detected integrated HPV sequences in the genomes of cervical cancer cell lines (Y Watanabe, H Yamamoto, F Itoh, and N Suzuki, unpubl.).

This study provides novel mechanistic insights into HBV-mediated hepatocarcinogenesis, which may have preventive and therapeutic applications for carriers of HBV and patients with HBV-HCC, as it suggests that epigenetic alterations provide candidate biochemical markers and therapeutic targets. This study, together with a recent global survey of HBV integration events (Ding et al. 2012; Fujimoto et al. 2012; Jiang et al. 2012; Sung et al. 2012; Toh et al. 2013), provides a foundation for the further experimentation and mechanistic understanding of HBV-HCC.

Methods

Cell lines and primary tissues

The PLC/PRF/5 (Alexander) human hepatoma cell line was obtained from the Japanese Collection of Research Bioresources (JCRB). HepG2.2.15 cells, kindly gifted by Professor Stephan Urban

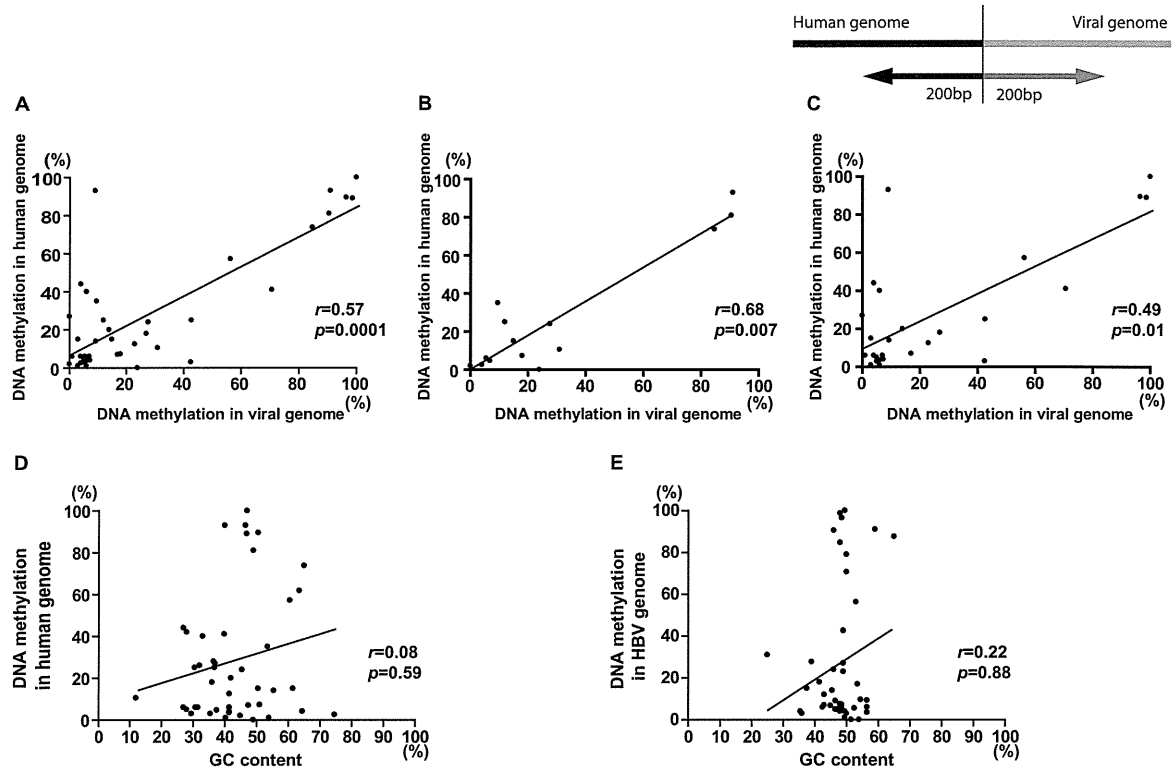

Figure 5. Correlation analysis between the methylation pattern of the integrated HBV DNA and that of the human genome. DNA fragments, including 200 bp of the HBV DNA and 200 bp of the human genome around the boundary, were analyzed for average methylation and GC content. (*A*) A correlation between the average methylation of the HBV DNA and that of the human genome in combined two cell lines and eight clinical samples ($n = 40$, $r = 0.57$, $P = 0.0001$, 95%CI = 0.3091–0.7545). (*B*) A correlation between the average methylation of the HBV DNA and that of the human genome in two cell lines ($n = 14$, $r = 068$, $P = 0.007$, 95%CI = 0.2233–0.8946). (*C*) A correlation between the average methylation of the HBV DNA and that of the human genome in eight clinical samples ($n = 26$, $r = 0.49$, $P = 0.01$, 95%CI = 0.1222–0.7463). (*D*) No correlation between the average methylation and GC contents in the human genome in the combined two cell lines and eight clinical samples ($n = 45$, $r = 0.08$, $P = 0.59$, 95%CI = −0.2253–0.3745). (*E*) No correlation between the average methylation and GC contents in the viral genome in the combined two cell lines and eight clinical samples ($n = 47$, $r = 0.22$, $P = 0.88$, 95%CI = −0.3151–0.2751).

at University Hospital Heidelberg, was derived from HepG2 cells transfected with a plasmid carrying four 5′-3′ tandem copies of the HBV genome (Koike et al. 1994). Cell lines were maintained in appropriate media containing 10% fetal bovine serum in plastic culture plates. Primary tissues from tumor and adjacent tissues were obtained at the time of the clinical procedures. Informed consent was obtained from all the patients before specimen collection. This study was approved by the institutional review board. DNA was extracted using the standard phenol–chloroform method. The concentration and quantity of extracted DNA were measured using a NanoDrop spectrophotometer (NanoDrop Technologies).

MCAM analysis

MCAM analysis was conducted as previously described (Oishi et al. 2012). A detailed protocol of MCA was previously described (Toyota et al. 1999). We used a custom human promoter array (G4426A-02212; Agilent Technologies) comprising 36,579 probes corresponding to 9021 unique genes. The probes on the array were selected to recognize SmaI/XmaI fragments mainly derived from sequences near gene transcription start sites. Five micrograms of genomic DNA was digested with 100 U of methylation-sensitive restriction endonuclease SmaI (New England Biolabs) for 24 h at 25°C, which cleaves unmethylated DNA leaving blunt ends (CCC/GGG). Subsequently, the DNA was digested with 20 U of methylation-insensitive restriction endonuclease XmaI for 6 h at 37°C, creating sticky ends (C/CCGGG). Five hundred milligrams of digested DNA was ligated using 50 μL of RMCA12 (5′-CCGGGCA GAAAG-3′)/RMCA24 (5′-CCACCGCCATCCGAGCCTTTCTGC-3′) primers and T4 DNA ligase (TaKaRa Bio) for 16 h at 16°C. After filling in the overhanging ends of the ligated DNA fragments at 72°C, the DNA was amplified for 5 min at 95°C followed by 25 cycles of 1-min incubation at 95°C and 3-min incubation at 77°C using 100 pmol of RMCA24 primer. MCA products were labeled with Cy5 (red) for DNA from hepatoma samples (both tumor and adjacent normal) and Cy3 (green) for DNA from human blood mixture of three healthy volunteers using a randomly primed Klenow polymerase reaction (Invitrogen) for 3 h at 37°C. Human CpG island arrays (4 × 44 K) were purchased from Agilent Technologies. Microarray protocols, including labeling, hybridization, and post-hybridization washing procedures, are provided at http://www.agilent.com/. Labeled samples were then hybridized to arrays in the presence of human Cot-1 DNA for 24 h at 65°C. After washing, arrays were scanned using an Agilent DNA microarray scanner and analyzed using Agilent Feature Extraction software (FE version 9.5.1.1, Agilent Technologies) at St. Marianna University School of Medicine. We used GeneSpring software (Agilent) for choosing candidate genes after normalization of the raw data.

DNA methylation analysis

Hidden Markov models have been successfully used to partition genomes into segments of comparable stochastic structure (Durbin et al. 1998). Using these models for sequence analysis performed

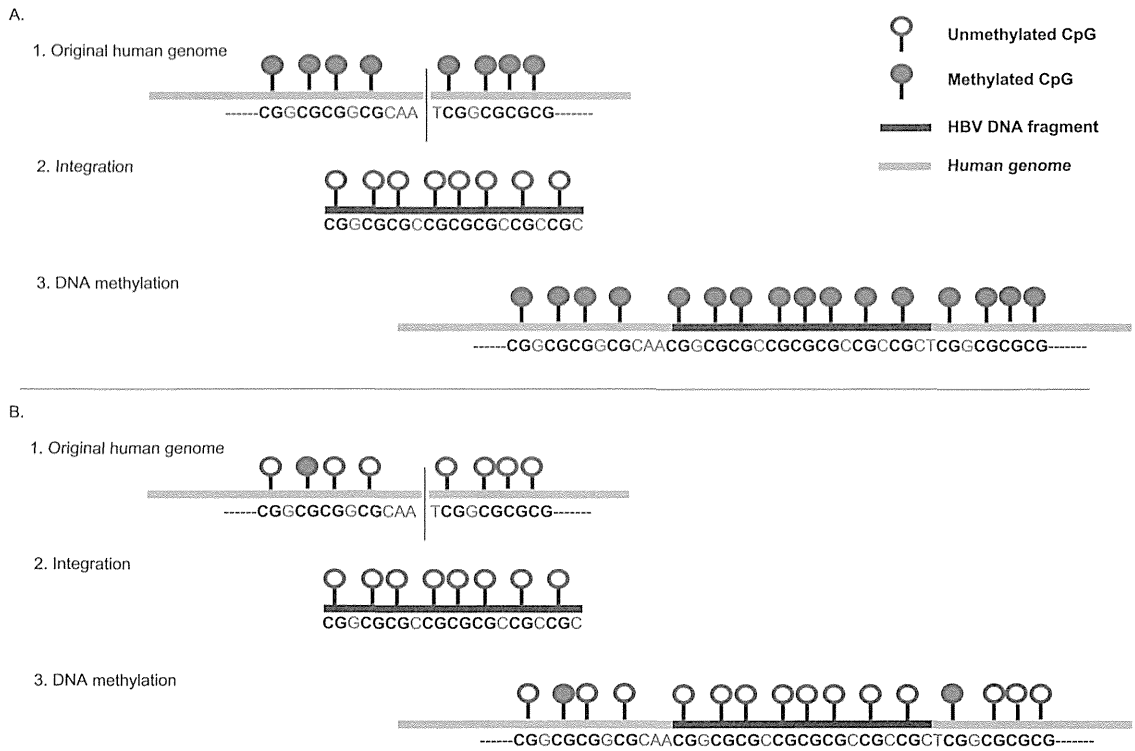

Figure 6. Schema of DNA methylation at HBV integrants and flanking human genomic sequences. (*A*) DNA hypermethylation was seen in both the integrated HBV fragment and human genome (original human genome shows dense methylation). The HBV genome often showed significant methylation when integrated into highly methylated host sites. (*B*) DNA hypermethylation was rarely seen in the integrated HBV fragment and human genome (original human genome shows low methylation). The HBV genome remained largely unmethylated when integrated into unmethylated host sites.

on the CpG plugin of bioinformatics software Geneious 5.5.8 (Biomatters), CpG islands were searched in the HBV genome (Kearse et al. 2012). Bisulfite PCR was performed using an EpiTect Bisulfite Kit (Qiagen) according to the manufacturer's protocol. One microliter of bisulfite-treated DNA was used as a template. The primers used for amplifying CpG sequences in the *HBx* gene are described in Supplemental Table 1. After PCR, the biotinylated strand was captured on streptavidin-coated beads (Amersham Bioscience) and incubated with sequencing primers (Supplemental Table 1). The pyrosequencing reactions were performed using the PyroMark Q24 and/or PyroMark Q24 advanced (Qiagen). Pyrosequencing quantitatively measures the methylation status of several CpG sites in a given sequence. These adjacent sites usually show highly concordant methylation. Therefore, the mean percentage of methylation at detected sites was used as a representative value for each sequence.

LINE1 and *Alu*Yb8 methylation analysis

The LINE1 and *Alu*Yb8 methylation levels, as measured by pyrosequencing, are good indicators of the cellular levels of 5-methylcytosine (i.e., the global DNA methylation level). To quantify relatively high LINE1 and *Alu*Yb8 methylation levels, we used pyrosequencing technology (Igarashi et al. 2010). PCR and subsequent pyrosequencing for LINE1 and *Alu*Yb8 were performed using the PyroMark kit (Qiagen). This assay amplifies a region of the LINE1 or *Alu*Yb8 elements that includes three CpG sites. The PCR was conducted as follows: 45 cycles for 20 sec at 95°C, for 20 sec at 50°C, and for 20 sec at 72°C, followed by 5 min at 72°C. The biotinylated PCR product was purified and converted to single strands to serve as a template for the pyrosequencing reaction using the pyrosequencing vacuum prep tool (Qiagen). The pyrosequencing reactions were performed using the PyroMark Q24 and/or PyroMark Q24 advanced (Qiagen). The percentage of Cs relative to the total sum of the Cs and Ts at each CpG site was calculated. The average of the percentages of Cs at the three CpG sites was used to represent the overall LINE1 and *Alu*Yb8 methylation levels in each sample.

FISH analysis of HBV integration

We developed a FISH analysis method to detect HBV DNA and demonstrate its presence in PLC/PRF/5 cells (Supplemental Fig. 3). The slides were pretreated with hydrogen peroxide and rinsed in 1× phosphate-buffered saline (PBS) to minimize background and quench endogenous peroxidase activity. To remove the excess cytoplasm, the slides were treated with pepsin and then fixed with 1% formaldehyde in PBS/$MgCl_2$. The slides were then dehydrated in an ethanol series (70%, 90%, and 100%) for 3 min at each step. The probes were designed based on the reference HBV sequence in PLC/PRF/5 DNA that is available from the Methylyzer 1.0 website (http://gbrowse.bioinfo.cnio.es/cgi-bin/VIRUS/HBV/). The FISH probes were prepared by combining the PCR-labeled probes (Supplemental Table 1), human Cot-1 DNA, and salmon sperm DNA. The probes were precipitated and mixed with hybridization buffer, and the probe DNA cocktail was denatured for 5 min at 95°C. The DNA on the slides was denatured by soaking in 70% formamide/2× SSC for 3 min at 74°C. The slides were immediately immersed in freshly prepared ice-cold 70% ethanol for 3 min, followed by 3-min immersions in 90% and then 100% ethanol. The denatured probe DNA was applied to the dry denatured slides and covered with a coverslip. The hybridization was performed for 16 h at 37°C.

Tyramide signal amplification (TSA)–FISH

TSA (tyramide signal amplification) detection kits were obtained from PerkinElmer. TSA-FISH detection was performed following the manufacturer's protocols with minor modifications. High stringency washes (0.1× SSC) were used to reduce the background, and TNT buffer (0.1 M Tris-HCl at pH 7.5, 0.15 M NaCl, 0.05% Tween 20) was adjusted to pH 7.0–7.5. The biotin- or DIG-labeled probes were detected using streptavidin-HRP or anti-DIG-HRP in TNB (0.1 M Tris-HCl at pH 7.5, 0.15 M NaCl, 0.05% blocking reagent [supplied in the kit]) for 30 min at room temperature and washed twice for 5 min each in TNT buffer. For the tyramide amplification procedure, the slide was covered with tyramide solution (Tyr-Bio, 1:50) for 10 min at room temperature. The tyramide solution was removed, and the slides were washed twice for 5 min each with TNT at room temperature. Fluorochrome-conjugated streptavidin (stAv-Alexa 488) diluted in TNB was used to detect the Tyr-Bio. The slides were incubated for 30 min at room temperature, washed with TNT buffer twice for 5 min each at room temperature, and covered with an anti-fade reagent containing DAPI (Speel et al. 1997; Schriml et al. 1999).

Identification of the chromosomal locations of viral–host junctions

The viral–host junctions were amplified using primers specific for human *Alu*Yb8 repetitive sequences and HBV X regions (Supplemental Table 1; Minami et al. 1995; Murakami et al. 2004). One microliter of genomic DNA solution served as a template in the subsequent PCR. We used touchdown PCR for most of the assays. All PCR assays included a denaturation step for 30 sec at 95°C, followed by an annealing step at various temperatures for 30 sec and an extension step for 30 sec at 72°C. PCR products were analyzed using electrophoresis through 1% agarose gels. PCR products were ligated to pCR-XL-TOPO vector DNA (TOPO XL PCR Cloning kit; Invitrogen) and transformed into competent cells. Positive colonies were selected and isolated using a QIA prep Spin Miniprep Kit (Qiagen). Direct sequence analysis of TOPO-TA cloning products was performed using a 3130 genetic analyzer (Applied Biosystems) (Watanabe et al. 2011). All sequences were searched for matches with HBV and pCR-XL-TOPO sequences using Geneious 5.5.8 (Biomatters) sequence analysis and assembly software and the BLAST program available on the UCSC Genome Browser (http://genome.ucsc.edu/).

Analysis of HBV DNA integration site sequences using NGS

Agilent's SureSelect target enrichment system is a highly efficient hybrid selection technique for optimizing NGS. We used this system and 12,391 custom baits covering the DNA sequences of HBV genotypes A to J and PLC/PRF/5 HBV sequences and optimized experiments for a GS FLX Titanium system (Roche). PLC/PRF/5, HepG2.2.15, and four paired tumor and nontumor samples (sample nos. 7, 8, 9, and 10 in Fig. 1B) were analyzed.

DNA methylation analysis of the integrated HBV genome as well as the adjacent human genome

DNA methylation was analyzed using bisulfite pyrosequencing (Oishi et al. 2012). The pyrosequencing reactions were performed using the PyroMark Q24 and/or PyroMark Q24 advanced (Qiagen). PLC/PRF/5, HepG2.2.15, and four paired tumor and nontumor samples (sample nos. 7, 8, 9, and 10 in Fig. 1B) were analyzed. Primers for methylation analysis of integration sites in PLC/PRF/5 are shown in Supplemental Table 1.

DNA methylation analysis of orthologous loci

Methylation levels of orthologous loci in HepG2.2.15 cells and in PBLs of a healthy volunteer at the same (empty) target sites of PLC/PRF/5 cells were analyzed using bisulfite pyrosequencing. Similarly, methylation levels of orthologous loci in PLC/PRF/5 cells and in PBLs at the same (empty) target sites of HepG2.2.15 cells were analyzed.

Allele-specific DNA methylation analysis of the integrated HBV genome as well as the adjacent human genome

Allele-specific DNA methylation was analyzed as described previously (Yamada and Ito 2011). The pyrosequencing reactions were performed using the PyroMark Q24 and/or PyroMark Q24 advanced (Qiagen).

Correlation analysis between the methylation pattern of the integrated HBV DNA and that of the human genome

DNA fragments, including 200 bp of the integrated HBV DNA and 200 bp of the human genome around the boundary, were analyzed for average methylation, GC content, and repetitive sequences in cell lines and clinical samples. RepeatMasker was used to identify repetitive elements in genomic sequences (AFA Smit, R Hubley, P Green, unpubl.). The Spearman correlation coefficient was used to assess correlations between the average methylation of the HBV DNA and that of the human genome. Correlations between GC content or repetitive sequences in the HBV DNA and the human genome were analyzed by using the Spearman correlation coefficient for continuous variables, and $P < 0.05$ was considered significant. All statistical analyses were performed using PRISM software for Windows, version 4 (GraphPad Prism).

Chromatin structure at the integrated HBV site

Using Bander software (Cheung et al. 2001; Furey and Haussler 2003), we analyzed the chromatin structure at the integrated HBV site in PLC/PRF/5 and HepG2.2.15.

Data access

All raw sequence data from this study have been submitted to the DDBJ Japanese Genotype-phenotype Archive (JGA; http://trace.ddbj.nig.ac.jp/jga/index_e.html) under accession number JGAS00000000015. Array data have been submitted to the NCBI Gene Expression Omnibus (GEO; http://www.ncbi.nlm.nih.gov/geo/) under accession number GSE59405.

Acknowledgments

We thank Drs. K. Watashi and T. Wakita for cell lines and Drs. T. Takayama, K. Takasaki, and S. Kawasaki for clinical samples. We also thank Drs. N. Matsumoto and N. Yamada-Ohkawa, as well as other members of the laboratory, for advice and suggestions. A part of the data used for this research was originally obtained by a research project of Hiroyuki Yamamoto and Yoshiyuki Watanabe led by Professor Fumio Itoh and is available at the website of the NBDC/JST (http://biosciencedbc.jp/en/). This work was supported in part by the Japan Society for the Promotion of Science (JSPS) Grants-in-Aid for Scientific Research (JSPS KAKENHI grant no. 23590964 to H. Yotsuyanagi).

Author contributions: Y.W. conceived the study, designed and performed the experiments, analyzed the data, and wrote the manuscript. H. Yamamoto designed the experiments, analyzed the data and wrote the manuscript. R.O. performed the experiments

and analyzed the data. M.T. provided intellectual support. M.Y., N.K., S.T., and A.S. provided clinical samples. H. Yotsuyanagi designed the experiments, analyzed the data and wrote the manuscript. K.K. provided intellectual support. F.I. supervised all aspects of the study.

References

Adey A, Burton JN, Kitzman JO, Hiatt JB, Lewis AP, Martin BK, Qiu R, Lee C, Shendure J. 2013. The haplotype-resolved genome and epigenome of the aneuploid HeLa cancer cell line. *Nature* **500:** 207–211.

Burgers WA, Blanchon L, Pradhan S, de Launoit Y, Kouzarides T, Fuks F. 2007. Viral oncoproteins target the DNA methyltransferases. *Oncogene* **26:** 1650–1655.

Cheung VG, Nowak N, Jang W, Kirsch IR, Zhao S, Chen XN, Furey TS, Kim UJ, Kuo WL, Olivier M, et al. 2001. Integration of cytogenetic landmarks into the draft sequence of the human genome. *Nature* **409:** 953–958.

Ding D, Lou X, Hua D, Yu W, Li L, Wang J, Gao F, Zhao N, Ren G, Li L, et al. 2012. Recurrent targeted genes of hepatitis B virus in the liver cancer genomes identified by a next-generation sequencing-based approach. *PLoS Genet* **8:** e1003065.

Doerfler W. 2008. In pursuit of the first recognized epigenetic signal-DNA methylation: a 1976 to 2008 synopsis. *Epigenetics* **3:** 125–133.

Doerfler W, Remus R, Müller K, Heller H, Hohlweg U, Schubbert R. 2001. The fate of foreign DNA in mammalian cells and organisms. *Dev Biol* **106:** 89–97.

Durbin R, Eddy S, Krogh A, Mitchison G. 1998. *Biological sequence analysis.* Cambridge University Press, Cambridge, UK.

Fernandez AF, Rosales C, Lopez-Nieva P, Graña O, Ballestar E, Ropero S, Espada J, Melo SA, Lujambio A, Fraga MF, et al. 2009. The dynamic DNA methylomes of double-stranded DNA viruses associated with human cancer. *Genome Res* **19:** 438–451.

Fujimoto A, Totoki Y, Abe T, Boroevich KA, Hosoda F, Nguyen HH, Aoki M, Hosono N, Kubo M, Miya F, et al. 2012. Whole-genome sequencing of liver cancers identifies etiological influences on mutation patterns and recurrent mutations in chromatin regulators. *Nat Genet* **44:** 760–764.

Furey TS, Haussler D. 2003. Integration of the cytogenetic map with the draft human genome sequence. *Hum Mol Genet* **12:** 1037–1044.

Gatza ML, Chandhasin C, Ducu RI, Marriott SJ. 2005. Impact of transforming viruses on cellular mutagenesis, genome stability, and cellular transformation. *Environ Mol Mutagen* **45:** 304–325.

Hilleman MR. 2004. Strategies and mechanisms for host and pathogen survival in acute and persistent viral infections. *Proc Natl Acad Sci* **101:** 14560–14566.

Igarashi S, Suzuki H, Niinuma T, Shimizu H, Nojima M, Iwaki H, Nobuoka T, Nishida T, Miyazaki Y, Takamaru H, et al. 2010. A novel correlation between LINE-1 hypomethylation and the malignancy of gastrointestinal stromal tumors. *Clin Cancer Res* **16:** 5114–5123.

Jiang Z, Jhunjhunwala S, Liu J, Haverty PM, Kennemer MI, Guan Y, Lee W, Carnevali P, Stinson J, Johnson S, et al. 2012. The effects of hepatitis B virus integration into the genomes of hepatocellular carcinoma patients. *Genome Res* **22:** 593–601.

Kan Z, Zheng H, Liu X, Li S, Barber TD, Gong Z, Gao H, Hao K, Willard MD, Xu J, et al. 2013. Whole-genome sequencing identifies recurrent mutations in hepatocellular carcinoma. *Genome Res* **23:** 1422–1433.

Kearse M, Moir R, Wilson A, Stones-Havas S, Cheung M, Sturrock S, Buxton S, Cooper A, Markowitz S, Duran C, et al. 2012. Geneious Basic: an integrated and extendable desktop software platform for the organization and analysis of sequence data. *Bioinformatics* **28:** 1647–1649.

Kim CM, Koike K, Saito I, Miyamura T, Jay DG. 1991. HBx gene of hepatitis B virus induces liver cancer in transgenic mice. *Nature* **351:** 317–320.

Koike K, Moriya K, Iino S, Yotsuyanagi H, Endo Y, Miyamura T, Kurokawa K. 1994. High-level expression of hepatitis B virus HBx gene and hepatocarcinogenesis in transgenic mice. *Hepatology* **19:** 810–819.

Lau C-C, Sun T, Ching AK, He M, Li JW, Wong AM, Co NN, Chan AW, Li PS, Lung RW, et al. 2014. Viral-human chimeric transcript predisposes risk to liver cancer development and progression. *Cancer Cell* **25:** 335–349.

Li S, Mao M. 2013. Next generation sequencing reveals genetic landscape of hepatocellular carcinomas. *Cancer Lett* **340:** 247–253.

Lupberger J, Hildt E. 2007. Hepatitis B virus–induced oncogenesis. *World J Gastroenterol* **13:** 74–81.

Minami M, Poussin K, Brechot C, Paterlini P. 1995. A novel PCR technique using *Alu*-specific primers to identify unknown flanking sequences from the human genome. *Genomics* **29:** 403–408.

Mirabello L, Sun C, Ghosh A, Rodriguez AC, Schiffman M, Wentzensen N, Hildesheim A, Herrero R, Wacholder S, Lorincz A, et al. 2012. Methylation of human papillomavirus type 16 genome and risk of cervical precancer in a Costa Rican population. *J Natl Cancer Inst* **104:** 556–565.

Murakami Y, Minami M, Daimon Y, Okanoue T. 2004. Hepatitis B virus DNA in liver, serum, and peripheral blood mononuclear cells after the clearance of serum hepatitis B virus surface antigen. *J Med Virol* **72:** 203–214.

Nakagawa H, Shibata T. 2013. Comprehensive genome sequencing of the liver cancer genome. *Cancer Lett* **340:** 234–240.

Oishi Y, Watanabe Y, Yoshida Y, Sato Y, Hiraishi T, Oikawa R, Maehata T, Suzuki H, Toyota M, Niwa H, et al. 2012. Hypermethylation of Sox17 gene is useful as a molecular diagnostic application in early gastric cancer. *Tumour Biol* **33:** 383–393.

Orend G, Kuhlmann I, Doerfler W. 1991. Spreading of DNA methylation across integrated foreign (adenovirus type 12) genomes in mammalian cells. *J Virol* **65:** 4301–4308.

Schriml LM, Padilla-Nash HM, Coleman A, Moen P, Nash WG, Menninger J, Jones G, Ried T, Dean M. 1999. Tyramide signal amplification (TSA)-FISH applied to mapping PCR-labeled probes less than 1 kb in size. *Biotechniques* **27:** 608–613.

Sells MA, Chen ML, Acs G. 1987. Production of hepatitis B virus particles in Hep G2 cells transfected with cloned hepatitis B virus DNA. *Proc Natl Acad Sci* **84:** 1005–1009.

Speel EJ, Ramaekers FC, Hopman AH. 1997. Sensitive multicolor fluorescence in situ hybridization using catalyzed reporter deposition (CARD) amplification. *J Histochem Cytochem* **45:** 1439–1446.

Sung WK, Zheng H, Li S, Chen R, Liu X, Li Y, Lee NP, Lee WH, Ariyaratne PN, Tennakoon C, et al. 2012. Genome-wide survey of recurrent HBV integration in hepatocellular carcinoma. *Nat Genet* **44:** 765–769.

Taniguchi Y, Nosaka K, Yasunaga J, Maeda M, Mueller N, Okayama A, Matsuoka M. 2005. Silencing of human T-cell leukemia virus type I gene transcription by epigenetic mechanisms. *Retrovirology* **2:** 64.

Tao Q, Robertson KD. 2003. Stealth technology: how Epstein-Barr virus utilizes DNA methylation to cloak itself from immune detection. *Clin Immunol* **109:** 53–63.

Toh ST, Jin Y, Liu L, Wang J, Babrzadeh F, Gharizadeh B, Ronaghi M, Toh HC, Chow PK, Chung AY, et al. 2013. Deep sequencing of the hepatitis B virus in hepatocellular carcinoma patients reveals enriched integration events, structural alterations and sequence variations. *Carcinogenesis* **34:** 787–798.

Toyota M, Ho C, Ahuja N, Jair KW, Li Q, Ohe-Toyota M, Baylin SB, Issa JP. 1999. Identification of differentially methylated sequences in colorectal cancer by methylated CpG island amplification. *Cancer Res* **59:** 2307–2312.

Uozaki H, Fukayama M. 2008. Epstein-Barr virus and gastric carcinoma-viral carcinogenesis through epigenetic mechanisms. *Int J Clin Exp Pathol* **1:** 198–216.

Watanabe Y, Castoro RJ, Kim HS, North B, Oikawa R, Hiraishi T, Ahmed SS, Chung W, Cho MY, Toyota M, et al. 2011. Frequent alteration of MLL3 frameshift mutations in microsatellite deficient colorectal cancer. *PLoS ONE* **6:** e23320.

Yamada Y, Ito T. 2011. Highly efficient PCR assay to discriminate allelic DNA methylation status using whole genome amplification. *BMC Res Notes* **4:** 179.

Received March 8, 2014; accepted in revised form December 29, 2014.

Contents lists available at ScienceDirect

Toxicology and Applied Pharmacology

journal homepage: www.elsevier.com/locate/ytaap

Mitochondrial iron accumulation exacerbates hepatic toxicity caused by hepatitis C virus core protein

Yuichi Sekine [a], Konomi Ito [a], Haruna Watanabe [a], Takafumi Nakano [a], Kyoji Moriya [b], Yoshizumi Shintani [b], Shinjime Fujie [b], Takeya Tsutsumi [b], Hideyuki Miyoshi [b], Hidetake Fujinaga [b], Seiko Shinzawa [b], Kazuhiko Koike [b], Toshiharu Horie [a,*]

[a] Laboratory of Biopharmaceutics, Graduate School of Pharmaceutical Sciences, Chiba University, 1-8-1 Inohana, Chuo-ku, Chiba 260-8675, Japan
[b] Department of Internal Medicine, Graduate School of Medicine, The University of Tokyo, 7-3-1 Hongo, Bunkyo-ku, Tokyo 113-8655, Japan

ARTICLE INFO

Article history:
Received 8 September 2014
Revised 9 December 2014
Accepted 16 December 2014
Available online 27 December 2014

Keywords:
Ca^{2+} uniporter
Proton reaction
Reactive oxygen species
Ru360
Hepatitis C virus

ABSTRACT

Patients with long-lasting hepatitis C virus (HCV) infection are at major risk of hepatocellular carcinoma (HCC). Iron accumulation in the livers of these patients is thought to exacerbate conditions of oxidative stress. Transgenic mice that express the HCV core protein develop HCC after the steatosis stage and produce an excess of hepatic reactive oxygen species (ROS). The overproduction of ROS in the liver is the net result of HCV core protein-induced dysfunction of the mitochondrial respiratory chain. This study examined the impact of ferric nitrilacetic acid (Fe-NTA)-mediated iron overload on mitochondrial damage and ROS production in HCV core protein-expressing HepG2 (human HCC) cells (Hep39b cells). A decrease in mitochondrial membrane potential and ROS production were observed following Fe-NTA treatment. After continuous exposure to Fe-NTA for six days, cell toxicity was observed in Hep39b cells, but not in mock (vector-transfected) HepG2 cells. Moreover, mitochondrial iron (^{59}Fe) uptake was increased in the livers of HCV core protein-expressing transgenic mice. This increase in mitochondrial iron uptake was inhibited by Ru360, a mitochondrial Ca^{2+} uniporter inhibitor. Furthermore, the Fe-NTA-induced augmentation of mitochondrial dysfunction, ROS production, and cell toxicity were also inhibited by Ru360 in Hep39b cells. Taken together, these results indicate that Ca^{2+} uniporter-mediated mitochondrial accumulation of iron exacerbates hepatocyte toxicity caused by the HCV core protein.

Introduction

Hepatitis C virus (HCV) infection is a major cause of chronic liver disease. About 120–200 million people are infected with HCV, increasing their risk of developing chronic hepatitis, cirrhosis, and eventually hepatocellular carcinoma (HCC) (Ikeda et al., 1998; Nishioka et al., 1991). The HCV genome is approximately 9.6 kb in size and encodes a polyprotein of ~3000 amino acids. The large HCV polyprotein is cleaved by host and viral proteases to generate at least ten smaller proteins, including four structural proteins (one core protein, two envelope proteins, and the E1, E2, and p7 ion channels) (Bukh et al., 1995) and six non-structural proteins (NH2-NS2, NS3, NS4A, NS4B, NS5A, and NS5B-COOH) (Bartenschlager and Lohmann, 2000). These proteins participate in viral replication and also influence cellular functions of the host.

Oxidative stress is commonly observed following HCV infection and is caused by increased levels of cellular reactive oxygen species (ROS) or by changes in cellular antioxidant capacities (Choi and Ou, 2006; Oberley, 2002; Otani et al., 2005). In particular, HCV core protein is known to be closely associated with the mitochondria and causes the increase in host ROS production, lipid peroxidation (Lau et al., 1998; Moriya et al., 2001; Okuda et al., 2002) and mitochondrial Ca^{2+} uptake. HCV core protein also reduces GSH and NADPH concentrations and mitochondrial complex I activities. These undertakings ultimately disrupt mitochondrial membrane permeability and trigger mitochondrial dysfunction (Wang et al., 2010; Wang and Weinman, 2006). As mitochondrial function is the master regulator of cellular energy and apoptotic cell death, mitochondrial injury can culminate in metabolic deficits and steatohepatitis, further exacerbating cell injury and dysfunction.

Due to the relationship between chronic HCV infection and the development of HCC, numerous studies have attempted to identify the HCV proteins that are responsible for hepatocarcinogenesis. These studies indicate that the HCV core protein can promote the immortalization of primary human hepatocytes (Ray et al., 2000), whereas the non-

Abbreviations: HCV, hepatitis C virus; HCC, hepatocellular carcinoma; ROS, reactive oxygen species; Fe-NTA, ferric nitrilacetic acid; JC-1, 5,5′,6,6′-tetrachrolo-1,1′,3,3′-tetraethylbenzimidazoly-carbocyanine iodide; CCCP, carbonyl cyanide-m-chlorophenyl hydrazine; MTT, 3-(4,5-dimethylthiazol-2-yl)-2,5-diphenyltetrazolium bromide; HPF, hydroxyphenyl fluorescein; ANT, adenine nucleotide translocator; HRP, horseradish peroxidase; DMEM, Dulbecco's Modified Eagle's Medium; CL, chemiluminescence; TTBS, Tris-buffered saline/0.05% Tween 20; BSA, bovine serum albumin; Hep39b, HCV core protein-expressing HepG2; Hepswx, vector-transfected HepG2.

Corresponding author at: Faculty of Pharmaceutical Sciences, Teikyo Heisei University, 2-21-2 Nakano, Nakano-ku, Tokyo 164-8530, Japan. Fax: +81 3 5860 4237.
E-mail address: t.horie@thu.ac.jp (T. Horie).

http://dx.doi.org/10.1016/j.taap.2014.12.004
0041-008X/

structural proteins NS3 and NS4B can transform NIH 3T3 cells, either individually or in combination with Ha-ras (Park et al., 2000). Iron overload in the liver, which is associated with the genetic disorder hereditary hemochromatosis, has been thought to increase the risk of HCC by about 200-fold (Bonkovsky et al., 1997; Kowdley, 2004). For example, the livers of patients afflicted with HCV are characterized by the elevated expression of transferrin receptor 1 and hepcidin, both of which stimulate iron uptake into hepatocytes (Bonkovsky et al., 1997; Hayashi et al., 1994). In contrast, iron depletion (in the form of dietary iron restriction and/or phlebotomy) can improve hepatic inflammation and lower serum aminotransferase activity in HCV patients (Hayashi et al., 1994). Thus, a major precipitating factor for the pathogenesis of HCV-related liver disease has been attributed to the augmentation of oxidative stress following iron accumulation. However, no underlying cellular mechanism has yet been elucidated.

This study investigated the effect of iron exposure on mitochondrial dysfunction, ROS production and cell toxicity in human hepatoma cells stably expressing the HCV core protein (Hep39b cells). The underlying mechanism responsible for mitochondrial iron accumulation in Hep39b cells and in the livers of HCV core protein-expressing transgenic mice was also examined.

Materials and methods

Chemicals and reagents. Ferric nitrate nonahydrate, nitrilotriacetic acid (NTA), 5,5′,6,6′-tetrachrolo-1,1′,3,3′-tetraethylbenzimidazolylcarbocyanine iodide (JC-1), carbonyl cyanide-m-chlorophenyl hydrazine (CCCP) and G418 disulfate were from Sigma Aldrich (St. Louis, MO). MitoTracker® Red was from Invitrogen (Carlsbad, CA). $^{59}FeSO_4$ was from Perkin-Elmer (Waltham, MA). Ru360 was from Merck Millipore Japan (Tokyo, Japan). MTT [3-(4,5-dimethylthiazol-2-yl)-2,5-diphenyltetrazolium bromide] was from Wako Pure Chemical Industries, Ltd. (Osaka, Japan). Hydroxyphenyl fluorescein (HPF) was from Sekisui Medical Co., Ltd. (Tokyo, Japan). Adenine nucleotide translocator (ANT) goat polyclonal IgG, CCDC109A goat polyclonal IgG and horseradish peroxidase (HRP)-conjugated anti-goat IgG were from Santa Cruz Biotechnology, Inc. (Santa Cruz, CA). All chemicals and solvents were of analytical grade.

Preparation of Fe-NTA. The Fe-NTA complex was prepared as described by Awai et al. (1979). Briefly, ferric nitrate was dissolved in 1 N HCl to form a 50 mM solution, and NTA was dissolved in 1 N NaOH to form a 150 mM solution. Equal volumes of the two solutions were mixed just before the experiment, and the pH was adjusted to 7.4 with $NaHCO_3$.

Assessment of cytotoxicity. Cytotoxicity was assessed by the MTT assay. Briefly, Hep39b and Hepswx cells were seeded into 96 well culture plates at a density of 8.4×10^3 cells/well and were exposed to various concentrations of Fe-NTA the following day, the medium was replaced with fresh medium containing the same component every 24 h. In some conditions, cells were treated with 20 μM Ru360, a mitochondrial Ca^{2+} uniporter inhibitor, for 1 h prior to Fe-NTA exposure. After six days, the cell culture medium was replaced by 50 μl MTT solution (5 mg/ml MTT in phenol red-free Dulbecco's Modified Eagle's Medium (DMEM)), and the cells were incubated for 2 h at 37 °C. To dissolve the reduced MTT crystals, 200 μl isopropanol was added. The absorbance of the dye was measured at a wavelength of 570 nm, and the turbidity of the cells (background absorbance) was measured at a reference wavelength of 630 nm. The absorbance of the controls (Hepswx and Hep39b) was set at 100%, and cytotoxicity was calculated as the absorbance of the experimental sample relative to that of the control.

Assessment of ROS production. ROS production was first assessed by chemiluminescence (CL) analysis. Briefly, cells were seeded into 35 mm glass-bottomed dishes at a density of 2.5×10^5 cells/dish and exposed to 300 μM Fe-NTA the following day, the medium was replaced with fresh medium containing the same component every 24 h. In some cases, cells were treated with Ru360 for 1 h prior to Fe-NTA treatment. After five days, the cell culture medium was replaced with phenol red-free DMEM containing Fe-NTA and Ru360, and the dish was protected from light. The following day, spontaneous CL was measured using a single photoelectron counting system (CLD-10; Tohoku Electronic Industrial Co., Ltd., Sendai, Japan), as described previously (Maeda et al., 2010). Emission was expressed in counts/10 min/mg protein.

ROS production was also assessed using HPF as a fluorescent probe for the selective detection of hydroxyl radicals. Briefly, cells were seeded into 35 mm glass-bottomed dishes, as described for CL analysis. After 7 days, the cell culture medium was replaced with modified Hanks' balanced salt solution (HBSS) containing 10 mM HEPES, 1 mM $MgCl_2$, 2 mM $CaCl_2$ and 2.7 mM glucose (pH 7.4). Next, 10 μM HPF and 20 nM MitoTracker® Red (a fluorescent probe for the mitochondria) were added, and cells were incubated for 15 min at 37 °C. Images of HPF and MitoTracker® Red staining were obtained using a laser scanning confocal microscope (FV300; Olympus Optical Co., Ltd., Tokyo, Japan). The wavelengths (excitation/emission) for the detection of HPF (green) and MitoTracker® Red (red) were 488 nm/515 nm and 579 nm/599 nm, respectively.

Assessment of mitochondrial membrane potential. Measurement of mitochondrial membrane potential was performed using the JC-1 stain, a lipophilic cation fluorescent dye that accumulates in the mitochondria. At a low mitochondrial membrane potential, the JC-1 dye exists as a monomeric molecule and fluoresces green, whereas at a higher membrane potential the JC-1 dye forms polymeric aggregates and fluoresces red. A fall in the mitochondrial membrane potential is therefore indicated by a decrease in the ratio of red signal to green signal.

Cells were cultured in 96 well black culture plates at a density of 8.4×10^3 cells/well and exposed to various concentrations of Fe-NTA the following day, the medium was replaced with fresh medium containing the same component every 24 h. After six days, the culture medium was replaced with 200 μl JC-1 solution (10 μg/ml JC-1 in HBSS), and cells were incubated in the dark for 30 min at 37 °C. After washing twice with HBSS, the absorbance of the cells in each well was immediately measured using a fluorescence plate reader with the excitation and emission wavelengths set at 490 nm and 530 nm (green)/590 nm (red), respectively.

Animals. The production of transgenic mice expressing the HCV core protein has been described previously (Moriya et al., 2001). Briefly, the HCV core protein gene was placed downstream of a transcriptional regulatory region from the hepatitis B virus and introduced into C57BL/6 mouse embryos (Clea Japan, Tokyo, Japan). All of the animals were treated humanely in accordance with the guidelines issued by the National Institute of Health and all procedures described below were approved by the animal care committee of Chiba University.

Isolation of mouse liver mitochondria. The mouse liver mitochondrial fraction was prepared according to a previously described method (Masubuchi et al., 2002). Livers were isolated from two mice and placed in ice-cold buffer containing 250 mM sucrose, 10 mM HEPES–KOH, and 0.5 mM EGTA (pH 7.4). Livers were cut into small cubes with scissors in the same buffer and homogenized five times with a Potter homogenizer. The homogenates were diluted to 0.25 g liver/ml and were centrifuged at 770 ×*g* for 5 min at 4 °C. The resulting supernatant was decanted and further centrifuged at 9800 ×*g* for 10 min. The pellet was resuspended to yield a concentration of 0.5 g liver/ml in buffer containing 250 mM sucrose, 10 mM HEPES–KOH and 0.3 mM EGTA (pH 7.4), and centrifuged at 4500 ×*g* for 10 min. The pellet was resuspended to yield a concentration of 1 g liver/ml in the same buffer and centrifuged at 2000 ×*g* for 2 min, followed by further centrifugation at 4500 ×*g* for 8 min. The

final pellet was then resuspended in buffer containing 250 mM sucrose and 10 mM HEPES–KOH (pH 7.4) and used for further experiments.

Mitochondrial iron uptake. All experiments were conducted in a 30 °C water bath. After pre-incubation of the mitochondria in buffer containing 225 mM sucrose, 10 mM KCl, 5 mM $MgCl_2$, 5 mM KH_2PO_4, and 20 mM Tris–HCl (pH 7.4) for 1 min, Ru360 was added at a final concentration of 10 μM, $^{59}FeSO_4$ was added after 1 min, and the ^{59}Fe remaining in the mitochondria after 10 min was measured using a gamma counter.

Western blotting analysis. The mouse liver mitochondrial fraction (10 μg protein) was subjected to electrophoresis on a 12.5% polyacrylamide slab gel containing 0.1% sodium dodecyl sulfate and transferred onto an Immobilon-P Transfer Membrane filter (Millipore Corporation, Billerica, MA). The membrane was blocked for 1 h at room temperature with Tris-buffered saline/0.05% Tween 20 (TTBS) containing 3% bovine serum albumin (BSA) and probed overnight at 4 °C with the CCDC109A goat polyclonal IgG (1:200) against the Ca^{2+} uniporter and the ANT goat polyclonal IgG (1:1000). The membrane was then incubated for 1 h at room temperature with donkey anti-goat IgG-HRP (1:3333). All antibodies were diluted in TTBS containing 0.1% BSA. Immunoreactive bands were detected using a LAS-1000 imaging system (Fuji Film, Tokyo, Japan) and an enhanced CL system (GE Healthcare, Little Chalfont, Buckinghamshire, UK).

Statistical analysis. All data are represented as the mean ± the standard error (S.E.). Data were statistically analyzed by using one-way ANOVA followed by the Bonferroni test for multiple comparison. For comparison among two groups, two-tailed Student's t-test was adopted. Differences between means at the level of $P < 0.05$ were considered significant.

Results

Iron-induced cytotoxicity in HCV core protein-expressing HepG2 cells

The iron uptake system is perturbed in HCV-infected hepatocytes due to elevated expression of transferrin receptor 1. However, because of its hydrophobicity, Fe-NTA is taken up into the cell in a transferrin receptor 1-independent manner by passive diffusion. Fe-NTA is then converted into free Fe^{2+} by several types of esterases. Therefore, Fe-NTA was used in the current study to control for intrinsic differences in active iron uptake between HCV core protein-expressing HepG2 cells (Hep39b cells) and vector-transfected HepG2 cells (Hepswx cells). After treatment with Fe-NTA for six days, cytotoxicity was assessed using the MTT assay. Concentration-dependent cytotoxicity of Fe-NTA against Hep39b cells was observed. By contrast, no cytotoxicity was observed against control Hepswx cells at Fe-NTA concentrations of less than 1000 μM (Fig. 1). These data indicate that HCV core protein expression affects the susceptibility of hepatocytes to Fe-NTA-induced iron cytotoxicity.

Effect of iron accumulation on ROS production in HCV core protein-expressing versus control hepatocytes

To directly measure free radical formation, we took advantage of methodology for measuring spontaneous CL and compared the levels of CL in HCV core protein-expressing Hep39b and control Hepswx cells (Fig. 2a). As shown in Fig. 2a, spontaneous CL was significantly higher in Hep39b cells by approximately 156% compared with that in Hepswx cells (6015 versus 3856 arbitrary units; $P < 0.01$). In the presence of 300 μM Fe-NTA, iron-induced CL was also significantly higher in Hep39b cells relative to Hepswx cells (2.61-fold versus 1.54-fold increase; $P < 0.01$ and $P < 0.001$, respectively) (Fig. 2a).

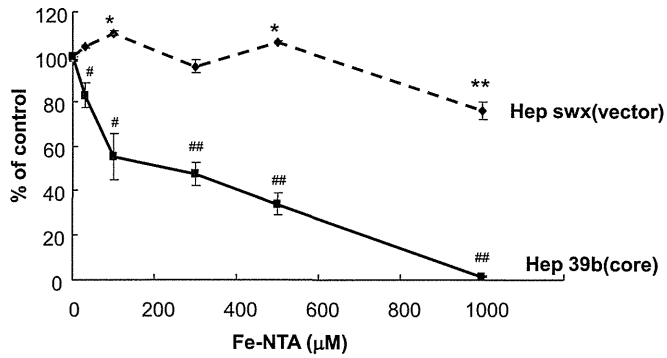

Fig. 1. Iron-induced cytotoxicity in control versus HCV core protein-expressing hepatocytes. Hepswx (dashed line) and Hep39b (solid line) cells were exposed with Fe-NTA (30, 100, 300, 500 and 1000 μM) for six days. Hepatotoxicity was determined using the MTT assay. Viability was calculated as the absorbance of the experimental sample relative to that of the controls (without Fe-NTA treatments). Values are the mean ± the S.E. $^{*}P < 0.05$ and $^{**}P < 0.01$, significantly different from the control (without Fe-NTA). $^{\#}P < 0.05$ and $^{\#\#}P < 0.01$, significantly different from respective control cells (Hepswx) ($n = 6$).

Effect of iron accumulation on mitochondrial ROS production

Mitochondria are a major source of ROS production. Therefore, we next examined the production of mitochondrial hydroxyl radicals by free iron catalyzation (i.e., the Fenton reaction). Since increased production of ROS was observed in Hep39b cells in the presence of Fe-NTA, we next examined mitochondrial ROS production by double staining with MitoTracker® Red (red), a fluorescent probe for the mitochondria, and HPF (green), a fluorescent probe for the selective detection of hydroxyl radicals. As shown in Fig. 2b, a strong fluorescent signal derived from HPF was observed in Hep39b cells in the presence of Fe-NTA. This fluorescence overlapped with that generated by MitoTracker® Red (Fig. 2b). The fluorescent signal derived from HPF in overlapped area was significantly higher in Hep39b cells by approximately 200% compared with that in Hepswx cells (Fig. 2c). These data indicate that mitochondrial hydroxyl radical production was increased in the presence of the HCV core protein and Fe-NTA.

Effect of HCV core protein on mitochondrial membrane potential

The HCV core protein is known to inhibit mitochondrial respiratory complex I activity (Korenaga et al., 2005). Inhibition of complex I leads to ROS formation due to premature electron leakage from the complex. Therefore, we next examined the effect of Fe-NTA on mitochondrial membrane potential in Hep39b cells by using JC-1, a lipophilic cationic dye that selectively enters the mitochondria and reversibly changes color from green to red as the membrane potential increases. Fig. 3 demonstrates that the mitochondrial membrane potential was decreased in HCV core protein-expressing Hep39b cells compared with control Hepswx cells. The decrease in membrane potential was significantly increased following exposure to Fe-NTA (300 and 1000 μM) for six days (Fig. 3).

Mitochondrial free iron uptake in HCV core protein-expressing versus control hepatocytes

Because mitochondrial hydroxyl radical production was increased in the presence of Fe-NTA (Fig. 2), the uptake of free iron into isolated mitochondria was next examined. To ensure a sufficient quantity and quality of the mitochondria for this experiment, mitochondria were isolated from the liver of HCV core protein-expressing transgenic and wild-type (control) mice. Fig. 4 shows that the concentration of mitochondrial free

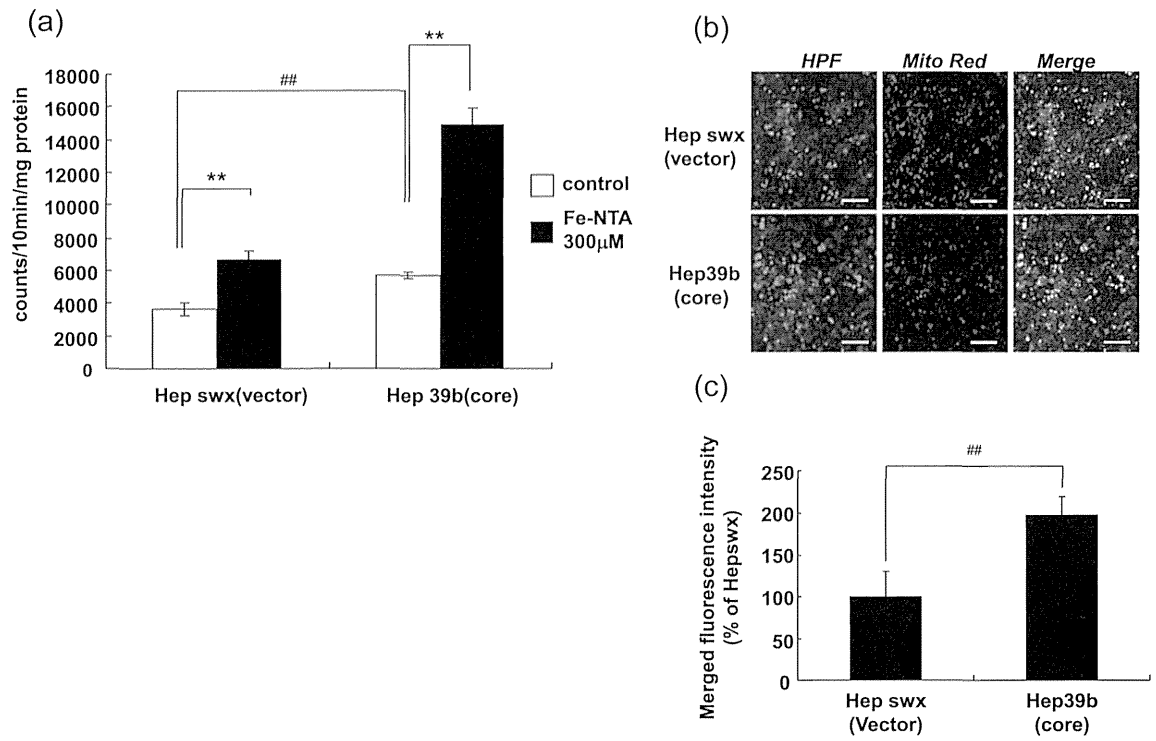

Fig. 2. Iron-induced mitochondrial ROS production is enhanced in HCV core protein-expressing hepatocytes. (a) Hepswx and Hep39b cells were exposed to Fe-NTA (300 μM) for six days. ROS production was determined using a CL analyzer. Detected counts were normalized by protein content of cell lysate. Values are given as the mean ± the S.E. $^{**}P < 0.01$ and $^{\#\#}P < 0.01$, significantly different from respective control (n = 3–4). (b) Hepswx and Hep39b cells were pretreated with HPF (green) and MitoTracker® Red (red). Mitochondrial ROS production was determined by the strength of yellow fluorescence in the merged pictures. The scale bar represents 100 μm. (c) Analysis of merged fluorescence microscopy images was done by ImageJ. Integrated density of merged area was automatically selected and fluorescence intensity of HPF was calculated within the merged area of 200–300 cells.

iron ($^{59}Fe^{2+}$) was significantly increased in the mitochondria derived from the transgenic versus the control mouse liver (62.2 ± 4.2 versus 79.5 ± 2.1 pmol/mg protein, respectively; $P < 0.05$), whereas the passive diffusion of $^{59}Fe^{2+}$ into the mitochondria (estimated by $^{59}Fe^{2+}$ uptake at 4 °C) was 31.1 ± 3.2 pmol/10 min/mg protein in Hepswx cells, and 29.2 ± 1.8 pmol/10 min/mg protein in Hep39b cells (not significantly different). Moreover, $^{59}Fe^{2+}$ uptake into the transgenic and control mitochondria was attenuated to the same level by Ru360 (48.2 ± 4.1 versus 47.5 ± 1.2 pmol/mg protein, respectively) (Fig. 4). These data indicate that calcium uniporter plays a role in free iron uptake into the mitochondria and that the activity of the Ca^{2+} uniporter is increased by the HCV core protein.

Effect of Ru360 on Fe-NTA-induced ROS production and cytotoxicity

We next examined the effect of Ru360 on Fe-NTA-induced ROS production and cytotoxicity in Hep39b versus Hepswx cells. As shown in Fig. 5a, in the absence of Fe-NTA, Ru360 had no effect on ROS production

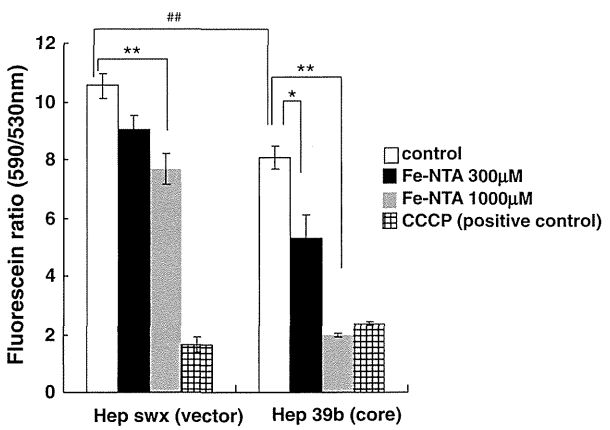

Fig. 3. The iron-induced reduction in mitochondrial membrane potential is increased by the expression of HCV core protein. Hepswx and Hep39b cells were exposed to Fe-NTA for six days. Mitochondrial membrane potential was estimated fluorometrically. Values are given as the mean ± the S.E. $^{*}P < 0.05$, $^{**}P < 0.01$ and $^{\#\#}P < 0.01$, significantly different from respective control (n = 6).

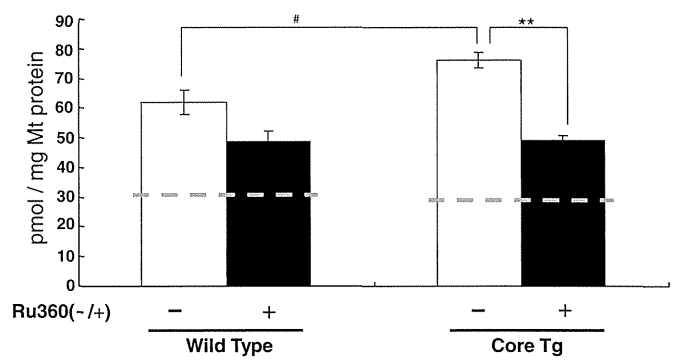

Fig. 4. Mitochondrial iron uptake is augmented by the expression of HCV core protein and inhibited by Ru360. Mitochondria were isolated from wild-type and HCV core protein transgenic (Tg) mice and exposed to $^{59}FeSO_4$ with/without Ru360. Free iron uptake was measured in the isolated mitochondria and the free iron uptake amount was normalized by mitochondrial protein content. The dashed line represents the passive diffusion into the mitochondria. Values are given as the mean ± the S.E. $^{**}P < 0.01$ and $^{\#}P < 0.05$, significantly different from respective control (n = 3–8).

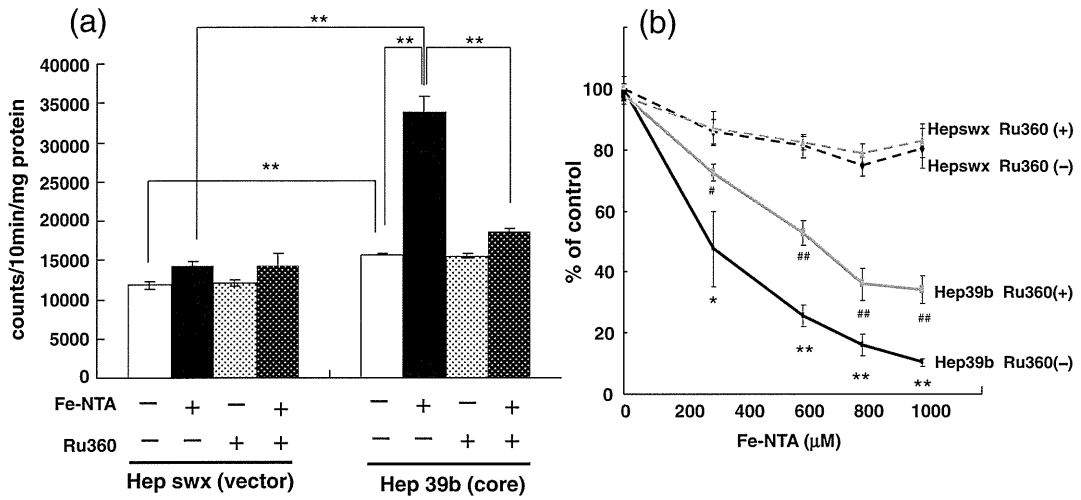

Fig. 5. Iron-induced ROS production and cytotoxicity are inhibited by Ru360 in HCV core protein-expressing hepatocytes. (a) Hepswx and Hep39b cells were exposed to Fe-NTA (300 μM) and Ru360 (20 μM) for six days. ROS production was determined using a CL analyzer. Values are given as the mean ± the S.E. $^{**}P < 0.01$, significantly different from respective control (n = 8). (b) Hepswx and Hep39b cells were exposed to Fe-NTA (300, 600, 800, and 1000 μM) and Ru360 (20 μM) for six days. Cytotoxicity was determined using the MTT assay. Values are given as the mean ± the S.E. $^{*}P < 0.05$ and $^{**}P < 0.01$, significantly different from Hepswx Ru360(−). $^{\#}P < 0.05$ and $^{\#\#}P < 0.01$, significantly different from Hep39b Ru360(−) (n = 6).

in Hepswx cells and Hep39b cells. On the other hand, Ru360 significantly suppressed Fe-NTA (300 μM)-induced ROS production in Hep39b but not Hepswx cells (Fig. 5a). Moreover, cytotoxicity following exposure to (300, 600, 800 and 1000 μM) Fe-NTA for six days was also specifically inhibited by Ru360 treatment in Hep39b cells (Fig. 5b).

Expression of the Ca^{2+} uniporter in isolated mitochondria

Given that mitochondrial free iron uptake is enhanced in HCV core protein-expressing Hep39b cells (Fig. 4), we next examined the expression of the Ca^{2+} uniporter in the mitochondria isolated from the liver of HCV core protein-expressing transgenic mice relative to control mice. As shown in Fig. 6, mitochondrial expression of the uniporter was similar in transgenic versus control mice, as assessed by Western blot analysis.

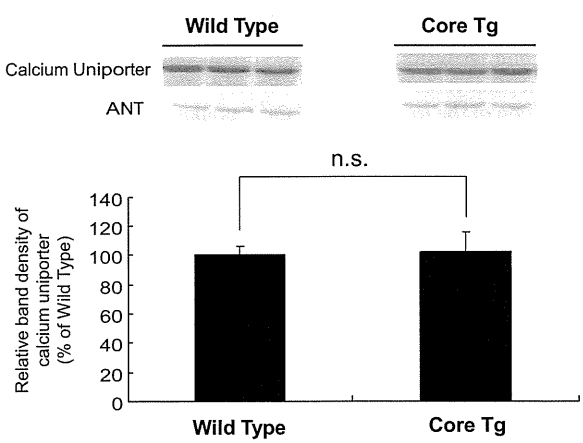

Fig. 6. Expression of mitochondrial Ca^{2+} uniporter in the livers of HCV core protein-expressing transgenic versus wild-type mice. Mitochondria were isolated from the livers of wild-type (control) and HCV core protein-expressing transgenic (Tg) mice. The expression levels of the Ca^{2+} uniporter and ANT (loading control) were determined by Western blot analysis. Mitochondrial proteins (10 μg) were loaded into each lane of the gel. The band density of the uniporter was normalized to the band density of ANT. Values are given as the mean ± the S.E. n.s.: not significantly different (n = 3).

Discussion

The accumulation of iron into the liver of HCV core protein-expressing transgenic mice fed a normal diet is similar to that observed in chronic HCV patients (Farinati et al., 1995; Kato et al., 2001). On the other hand, the expression level of hepcidin, which regulates iron metabolism by inhibiting iron absorption from the intestine and the hepatic portal system, is reportedly decreased in the liver of HCV patients and full-length HCV genome-expressing transgenic mice, but not in the liver of HCV core protein-expressing transgenic mice (Moriya et al., 2010; Muckenthaler, 2008). Therefore, although the precise regulation of iron transport into the mitochondria is essential for heme biosynthesis, hemoglobin production, and Fe–S clustering, the mechanism(s) behind mitochondrial iron homeostasis is not yet fully understood.

Previous work from our group revealed elevated ROS generation in HCV core protein-expressing transgenic mice (Moriya et al., 2001). Moreover, our previous work, along with that of others (Korenaga et al., 2005), showed that the core protein interacts with the outer mitochondrial membrane and impairs the mitochondrial respiratory chain in the normal mouse liver via inhibition of complex I activity (unpublished data). Inhibition of respiratory chain complexes ultimately leads to the overproduction of ROS via electron leakage from the mitochondria. Therefore, we hypothesized that the inducible mitochondrial iron transport system exacerbates hepatic toxicity caused by the HCV core protein.

This study employed Fe-NTA to exclude intrinsic differences in iron uptake into HCV core protein-expressing Hep39b cells and vector-transfected Hepswx cells. In addition, we demonstrated that HCV core protein-induced alterations in mitochondrial ROS production and membrane potential were augmented in the presence of iron (Figs. 2 and 3). These data may indicate that iron-dependent mitochondrial dysfunction was amplified via the Fenton reaction, which produces potent reactive free radicals (i.e., hydroxyl radicals) (Fig. 7).

Iron is absolutely essential for the sustenance of all forms of life due to its unusual ability to serve as both an electron donor and acceptor. On the other hand, free iron is also potentially toxic, which is related to its ability to donate and accept electrons within the cell. Free iron catalyzes the conversion of hydrogen peroxide into free radicals, which can cause damage to the mitochondria and cellular structures. For this reason, the iron homeostasis is strictly regulated, and the impairment of iron homeostasis is related to several diseases. In patients with HCV, hepatic

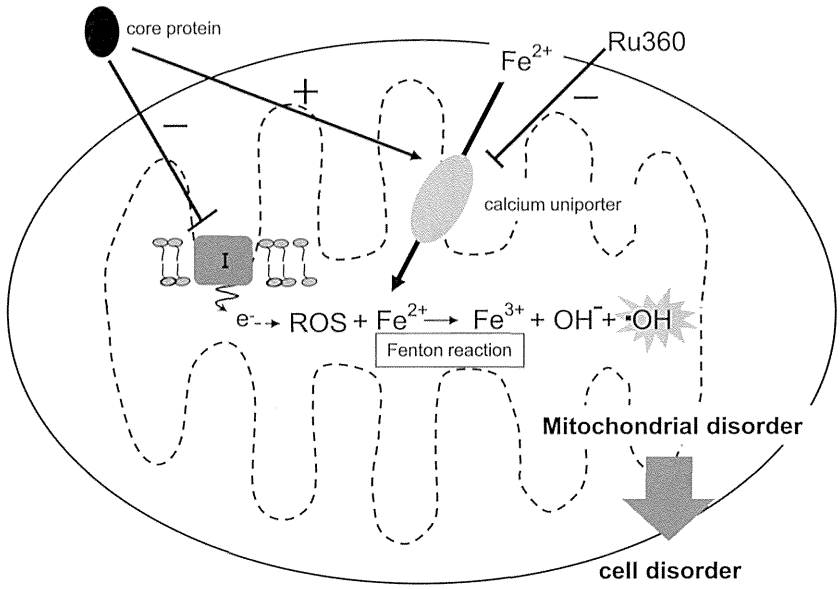

Fig. 7. Proposed mechanism of mitochondrial iron accumulation and hepatic cytotoxicity caused by the HCV core protein. The HCV core protein induces mitochondrial ROS production by inhibiting mitochondrial complex I. In addition, it is suggested that the HCV core protein stimulates mitochondrial iron uptake through the mitochondrial Ca^{2+} uniporter. The excess iron then leads to mitochondrial ROS production and mitochondrial/cellular malfunction/disorder when the HCV core protein is expressed.

and serum free iron concentrations are ~7-fold higher (12.5 mmol/g liver and 134 mg/dl, respectively) than those of a normal individual (Farinati et al., 1995; Kageyama et al., 1998; Olynyk et al., 1995; Silva et al., 2005). In this study, significant hepatotoxicity was observed at 30 μM Fe-NTA in HCV core protein-expressing Hep39b cells (Fig. 1). Therefore, a physiologically relevant concentration of iron (30 μM), which is not sufficient to induce cell toxicity by itself, was synergistic with the toxic actions of the core protein (Fig. 1). This interplay was similarly revealed by the synergy between iron and the core protein in inducing mitochondrial dysfunction and ROS production (Figs. 2 and 3).

This study further demonstrated that mitochondrial free iron uptake was partially mediated by the Ca^{2+} uniporter. The Ca^{2+} uniporter was selectively inhibited by Ru360 and exhibited an increased capacity to uptake iron into HCV core protein-expressing liver mitochondria versus normal liver mitochondria (Fig. 4). However, the expression of the uniporter was unaltered in core protein-expressing transgenic mice relative to normal mice (Fig. 6). Li et al. (2007) reported that the activity of the Ca^{2+} uniporter was up-regulated in the presence of the core protein: The in vitro incubation of mouse liver mitochondria with HCV core protein (100 ng/mg) increased the Ca^{2+} entry rate by ~2-fold. The Ca^{2+} uniporter is located in the inner mitochondrial membrane and transports not only Ca^{2+} but also other metal cationic ions (e.g., Fe^{2+}) into the mitochondrial matrix space in a mitochondrial membrane potential-dependent fashion (Bernardi, 1999).

Iron uptake was significantly suppressed to the same level by Ru360 in the mitochondria isolated from both core protein-expressing transgenic and normal mice (Fig. 4). Moreover, as free iron uptake into the mitochondria was still observed at 4 °C for both types of the mitochondria, about half of the iron (Hepswx; 31.1 ± 3.2 pmol/10 min/mg protein, Hep39b; 29.2 ± 1.8 pmol/10 min/mg protein) was estimated to enter into the mitochondria by passive diffusion (Fig. 4, dashed line). These data indicate that the up-regulation of iron uptake in the mitochondria isolated from transgenic mice was mediated by the HCV core protein-induced stimulation of Ru360-sensitive Ca^{2+} uniporter transport activity. However, the mechanism by which the core protein alters the function of the mitochondrial uniporter is still unclear, especially given that the core protein binds to the outer mitochondrial membrane, and the uniporter is located in the inner mitochondrial membrane. It is known that mitochondrial calcium uniporter possibly forms multi-molecular complex (Raffaello et al., 2012). Mitochondrial calcium uniporter function could be altered by the effect on essential regulator and/or protein involved in the assembly of the channel. In this regard, though our current study demonstrated that HCV core protein had no effect on Ca^{2+} uniporter expression (Fig. 6), it is possible that other mechanisms are involved in the HCV core protein-induced stimulation of Ca^{2+} uniporter transport activity. Further study should be addressed in the future.

Interferon-α has been used as monotherapy for chronic hepatitis C, yet only about 40–50% of hepatitis C patients experience an initial biochemical response to the cytokine. Interestingly, high iron accumulation in chronic HCV carriers is related to a poor response to interferon therapy (Walters et al., 1973). In addition, some investigators have suggested that iron removal therapy (via phlebotomy or food therapy (i.e., restriction of an iron rich-diet)) can attenuate liver damage in hepatitis C patients by still unknown mechanisms (Hayashi et al., 1994; Kato et al., 2007). The current study showed that the HCV core protein-induced mitochondrial iron uptake is responsible for exacerbating mitochondrial dysfunction and ROS production, which finally seems to lead to hepatocyte toxicity (Fig. 7). Based on these results, we suggest that inhibition of the mitochondrial Ca^{2+} uniporter may provide a new therapeutic approach to treat liver disease in HCV patients.

Conflict of interest statement

The authors declare no conflict of interest.

Acknowledgments

This work was supported by a grant-in-aid for scientific research (A) 548 (21249003) and a grant-in-aid for young scientists (B) (21790141) from the Ministry of Education, Culture, Sports, Science and Technology of Japan.

References

Awai, M., Narasaki, M., Yamanoi, Y., Seno, S., 1979. Induction of diabetes in animals by parenteral administration of ferric nitrilotriacetate. A model of experimental hemochromatosis. Am. J. Pathol. 95, 663–673.

Bartenschlager, R., Lohmann, V., 2000. Replication of hepatitis C virus. J. Gen. Virol. 81, 1631–1648.
Bernardi, P., 1999. Mitochondrial transport of cations: channels, exchangers, and permeability transition. Physiol. Rev. 79, 1127–1155.
Bonkovsky, H.L., Banner, B.F., Rothman, A.L., 1997. Iron and chronic viral hepatitis. Hepatology 25, 759–768.
Bukh, J., Miller, R.H., Purcell, R.H., 1995. Genetic heterogeneity of hepatitis C virus: quasispecies and genotypes. Semin. Liver Dis. 15, 41–63.
Choi, J., Ou, J.H., 2006. Mechanisms of liver injury. III. Oxidative stress in the pathogenesis of hepatitis C virus. Am. J. Physiol. Gastrointest. Liver Physiol. 290, G847–G851.
Farinati, F., Cardin, R., De Maria, N., Della Libera, G., Marafin, C., Lecis, E., et al., 1995. Iron storage, lipid peroxidation and glutathione turnover in chronic anti-HCV positive hepatitis. J. Hepatol. 22, 449–456.
Hayashi, H., Takikawa, T., Nishimura, N., Yano, M., Isomura, T., Sakamoto, N., 1994. Improvement of serum aminotransferase levels after phlebotomy in patients with chronic active hepatitis C and excess hepatic iron. Am. J. Gastroenterol. 89, 986–988.
Ikeda, K., Saitoh, S., Suzuki, Y., Kobayashi, M., Tsubota, A., Koida, I., et al., 1998. Disease progression and hepatocellular carcinogenesis in patients with chronic viral hepatitis: a prospective observation of 2215 patients. J. Hepatol. 28, 930–938.
Kageyama, F., Kobayashi, Y., Murohisa, G., Shimizu, E., Suzuki, F., Kikuyama, M., et al., 1998. Failure to respond to interferon-alpha 2a therapy is associated with increased hepatic iron levels in patients with chronic hepatitis C. Biol. Trace Elem. Res. 64, 185–196.
Kato, J., Kobune, M., Nakamura, T., Kuroiwa, G., Takada, K., Takimoto, R., et al., 2001. Normalization of elevated hepatic 8-hydroxy-2′-deoxyguanosine levels in chronic hepatitis C patients by phlebotomy and low iron diet. Cancer Res. 61, 8697–8702.
Kato, J., Miyanishi, K., Kobune, M., Nakamura, T., Takada, K., Takimoto, R., et al., 2007. Long-term phlebotomy with low-iron diet therapy lowers risk of development of hepatocellular carcinoma from chronic hepatitis C. J. Gastroenterol. 42, 830–836.
Korenaga, M., Wang, T., Li, Y., Showalter, L.A., Chan, T., Sun, J., et al., 2005. Hepatitis C virus core protein inhibits mitochondrial electron transport and increases reactive oxygen species (ROS) production. J. Biol. Chem. 280, 37481–37488.
Kowdley, K.V., 2004. Iron, hemochromatosis, and hepatocellular carcinoma. Gastroenterology 127, S79–S86.
Lau, J.Y., Xie, X., Lai, M.M., Wu, P.C., 1998. Apoptosis and viral hepatitis. Semin. Liver Dis. 18, 169–176.
Li, Y., Boehning, D.F., Qian, T., Popov, V.L., Weinman, S.A., 2007. Hepatitis C virus core protein increases mitochondrial ROS production by stimulation of Ca^{2+} uniporter activity. FASEB J. 21, 2474–2485.
Maeda, T., Miyazono, Y., Ito, K., Hamada, K., Sekine, S., Horie, T., 2010. Oxidative stress and enhanced paracellular permeability in the small intestine of methotrexate-treated rats. Cancer Chemother. Pharmacol. 65, 1117–1123.
Masubuchi, Y., Nakayama, S., Horie, T., 2002. Role of mitochondrial permeability transition in diclofenac-induced hepatocyte injury in rats. Hepatology 35, 544–551.
Moriya, K., Nakagawa, K., Santa, T., Shintani, Y., Fujie, H., Miyoshi, H., et al., 2001. Oxidative stress in the absence of inflammation in a mouse model for hepatitis C virus-associated hepatocarcinogenesis. Cancer Res. 61, 4365–4370.
Moriya, K., Miyoshi, H., Shinzawa, S., Tsutsumi, T., Fujie, H., Goto, K., et al., 2010. Hepatitis C virus core protein compromises iron-induced activation of antioxidants in mice and HepG2 cells. J. Med. Virol. 82, 776–792.
Muckenthaler, M.U., 2008. Fine tuning of hepcidin expression by positive and negative regulators. Cell Metab. 8, 1–3.
Nishioka, K., Watanabe, J., Furuta, S., Tanaka, E., Iino, S., Suzuki, H., et al., 1991. A high prevalence of antibody to the hepatitis C virus in patients with hepatocellular carcinoma in Japan. Cancer 67, 429–433.
Oberley, T.D., 2002. Oxidative damage and cancer. Am. J. Pathol. 160, 403–408.
Okuda, M., Li, K., Beard, M.R., Showalter, L.A., Scholle, F., Lemon, S.M., et al., 2002. Mitochondrial injury, oxidative stress, and antioxidant gene expression are induced by hepatitis C virus core protein. Gastroenterology 122, 366–375.
Olynyk, J.K., Reddy, K.R., Di Bisceglie, A.M., Jeffers, L.J., Parker, T.I., Radick, J.L., et al., 1995. Hepatic iron concentration as a predictor of response to interferon alfa therapy in chronic hepatitis C. Gastroenterology 108, 1104–1109.
Otani, K., Korenaga, M., Beard, M.R., Li, K., Qian, T., Showalter, L.A., et al., 2005. Hepatitis C virus core protein, cytochrome P450 2E1, and alcohol produce combined mitochondrial injury and cytotoxicity in hepatoma cells. Gastroenterology 128, 96–107.
Park, J.S., Yang, J.M., Min, M.K., 2000. Hepatitis C virus nonstructural protein NS4B transforms NIH3T3 cells in cooperation with the Ha-ras oncogene. Biochem. Biophys. Res. Commun. 267, 581–587.
Raffaello, A., De Stefani, D., Rizzuto, R., 2012. The mitochondrial Ca^{2+} uniporter. Cell Calcium 52, 16–21.
Ray, R.B., Meyer, K., Ray, R., 2000. Hepatitis C virus core protein promotes immortalization of primary human hepatocytes. Virology 271, 197–204.
Silva, I.S., Perez, R.M., Oliveira, P.V., Cantagalo, M.I., Dantas, E., Sisti, C., et al., 2005. Iron overload in patients with chronic hepatitis C virus infection: clinical and histological study. J. Gastroenterol. Hepatol. 20, 243–248.
Walters, G.O., Miller, F.M., Worwood, M., 1973. Serum ferritin concentration and iron stores in normal subjects. J. Clin. Pathol. 26, 770–772.
Wang, T., Weinman, S.A., 2006. Causes and consequences of mitochondrial reactive oxygen species generation in hepatitis C. J. Gastroenterol. Hepatol. 21 (Suppl. 3), S34–S37.
Wang, T., Campbell, R.V., Yi, M.K., Lemon, S.M., Weinman, S.A., 2010. Role of hepatitis C virus core protein in viral-induced mitochondrial dysfunction. J. Viral Hepat. 17, 784–793.

Hepatology Research

Hepatology Research 2014 doi: 10.1111/hepr.12361

Original Article

Potential associations between perihepatic lymph node enlargement and liver fibrosis, hepatocellular injury or hepatocarcinogenesis in chronic hepatitis B virus infection

Masaya Sato,[1,2] Hiromi Hikita,[1] Shu Hagiwara,[1] Mamiko Sato,[1] Yoko Soroida,[1] Atsushi Suzuki,[1] Hiroaki Gotoh,[1] Tomomi Iwai,[1] Soichi Kojima,[3] Tomokazu Matsuura,[4] Hiroshi Yotsuyanagi,[5] Kazuhiko Koike,[2] Yutaka Yatomi[1] and Hitoshi Ikeda[1]

Departments of [1]Clinical Laboratory Medicine, [2]Gastroenterology and [5]Infectious Disease, Graduate School of Medicine, The University of Tokyo, [4]Department of Laboratory Medicine, The Jikei University School of Medicine, Tokyo, and [3]Regulation Technology Unit, RIKEN Center for Life Science Technologies, Wako, Saitama, Japan

Aim: Although perihepatic lymph node enlargement (PLNE) is frequently observed in chronic liver disease, little is known about PLNE in chronic hepatitis B virus (HBV) infection. We aimed to evaluate this issue.

Methods: We originally enrolled a consecutive 502 patients with chronic HBV infection. Among them, 288 patients without history of interferon-based or nucleoside analog treatment and hepatocellular carcinoma (HCC) were primarily analyzed.

Results: PLNE was detected in 27 of 288 (9.4%) patients, which was fewer than that in chronic hepatitis C patients but more than that in subjects undertaking a general health examination as previously reported. The presence of PLNE was significantly associated with a higher probability of having an aspartate aminotransferase (AST) platelet ratio index of more than 1.5 (11.1% vs 1.5%, $P = 0.01$), a higher AST level (38.0 vs 26.8 U/L, $P = 0.001$), a higher alanine aminotransferase level (50.1 vs 28.0 U/L, $P < 0.0001$), and a lower platelet count (18.6 vs 20.6 $\times$ $10^4/\mu$L, $P = 0.048$) after adjustment for sex and age. However, in our original sample ($n = 502$), PLNE was observed in 1.4% of the patients with HCC and/or its history whereas 9.2% of the patients without HCC, and the proportion was significantly lower in patients with HCC and/or its history ($P = 0.03$).

Conclusion: PLNE was associated with liver fibrosis and hepatocellular injury, but was negatively associated with HCC in chronic HBV infection.

Key words: fibrosis, hepatitis B, immune response, inflammatory activity, perihepatic lymph node enlargement

INTRODUCTION

HEPATITIS B VIRUS (HBV) infection is an important cause of chronic liver disease globally, with an estimated 350 million carriers worldwide.[1] Chronic HBV infection is a major risk factor for several liver diseases, such as chronic hepatitis B (CHB), liver cirrhosis and hepatocellular carcinoma (HCC),[2] which is the fifth most common cancer worldwide.[3] HBV infection itself is non-cytopathic, and it is the immune response to the viral antigens that are thought to be responsible for the necroinflammatory process involved in chronic infection, cirrhosis and HCC.[4]

Perihepatic lymph node enlargement (PLNE) is frequently observed in patients with chronic liver disease,[5] especially in those with hepatitis C virus (HCV) infection.[6,7] Although some studies have reported that PLNE was associated with inflammatory activity, stage of liver fibrosis or hepatitis viral load,[7–12] such associations were inconsistent among other studies,[6–8,10–15] suggesting that the clinical significance of PLNE in HCV infection has not been fully established yet. We have recently reported that PLNE is negatively associated with the response to interferon (IFN)-based treatment or development of HCC in patients with chronic hepatitis C (CHC).[16,17] It is

Correspondence: Dr Hitoshi Ikeda, Department of Clinical Laboratory Medicine, Graduate School of Medicine, The University of Tokyo, 7-3-1 Hongo, Bunkyo-ku, Tokyo 113-8655, Japan. Email: ikeda-1im@h.u-tokyo.ac.jp

Conflict of interest: None of the authors have any conflicts of interest.

Received 11 November 2013; revision 3 April 2014; accepted 15 May 2014.